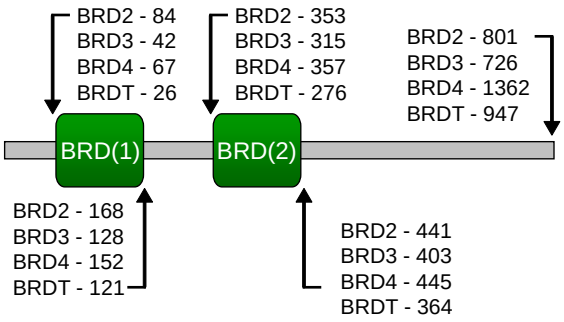

Supplementary Figure 1 | Domain boundaries of the BET sub-family of human bromodomains. Sequence boundaries for recombinant bromodomains utilized for biochemical and structural studies are shown.

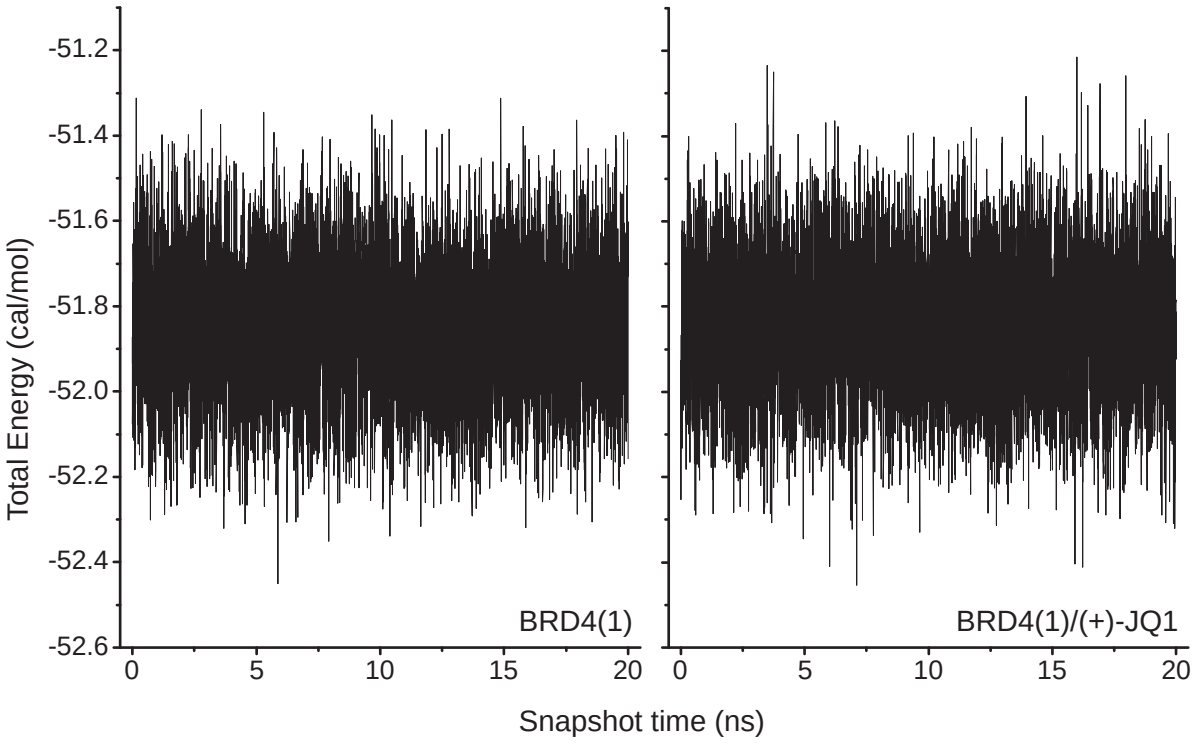

Supplementary Figure 2 | Total energy (ETOT) of bromodomains with JQ1 over time by molecular dynamics. The total energy of BRD4(1) (left) and BRD4(1) with (+)-JQ1 (right) over 20 ns simulation time is presented.

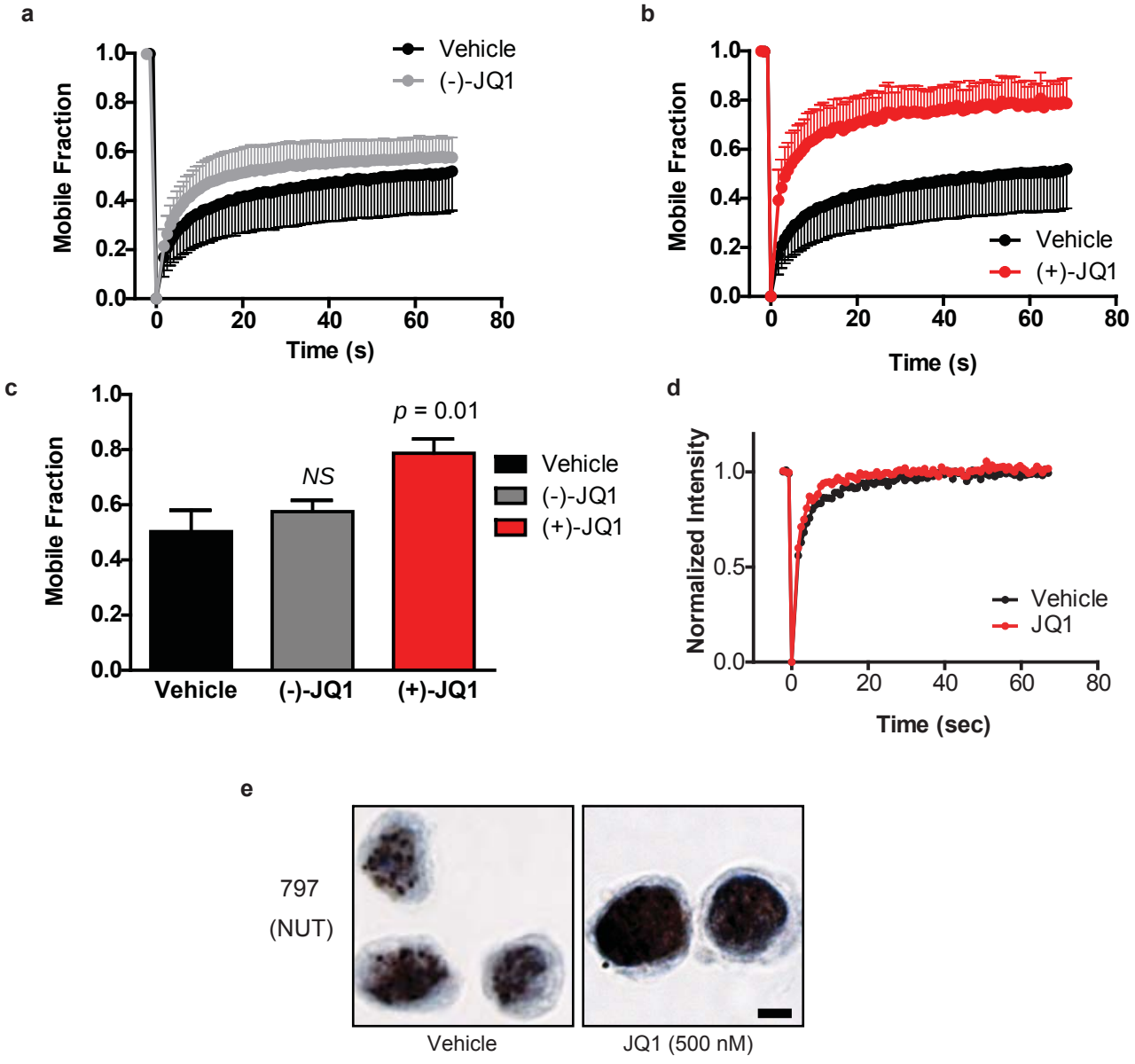

Supplementary Figure 3 | The (-)-JQ1 enantiomer does not bind competitively to BRD4-NUT in cells, while (+)-JQ1 displaces BRD4-NUT but not NUT. a, BRD4 is unaffected by the presence of (-)-JQ1 (250 nM, 5 h) compared to vehicle control. Data represent the mean ± s.d. (n = 5). b, Expressed GFP-BRD4 demonstrates enhanced recovery in the presence of (+)-JQ1 (250 nM, 5 h), in a parallel comparative study. Data represent the mean ± s.d. (n = 5). c, Quantitative comparison of the mobile fraction of GFP-BRD4 observed in FRAP studies (a, b). Data represent the mean ± s.d. (n = 5) and are annotated with p-values as obtained from a two-tailed t-test comparing ligand treated samples to vehicle controls. d, FRAP of GFP-NUT is unaffected by the presence of (+)-JQ1 (250 nM) compared to vehicle control. e, JQ1 (500 nM, 48 h) prompts a loss of focal nuclear staining for NUT (anti-NUT; 100x; scale bar is 10 μm).

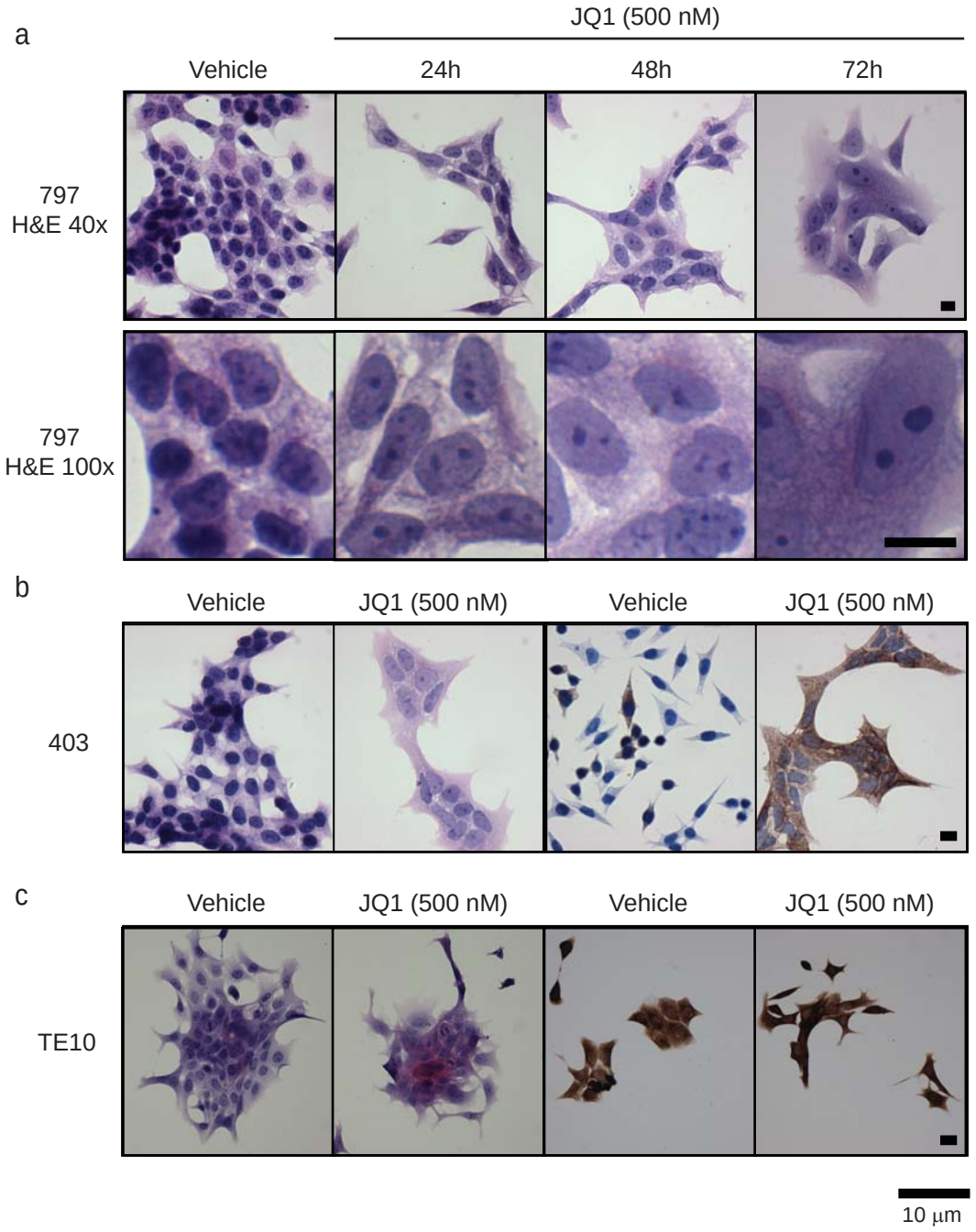

Supplementary Figure 4 | JQ1 selectively induces squamous differentiation in NUT midline carcinoma. a, NMC 797 cells treated with JQ1 (500 nM) demonstrate time-dependent cytologic signs of squamous differentiation (H&E; 40x and 100x, as shown), exemplified by cell spindling, flattening and the development of open chromatin. b, NMC Per403 cells treated with JQ1 (500 nM, 48 h) exhibit comparable signs of squamous differentiation. Cell spindling and cytosolic keratinization is illustrated by H&E and keratin staining, respectively (40x). c, The non-NMC squamous carcinoma cell line TE10 fails to differentiate in response to JQ1 (500 nM), illustrated by H&E and keratin (AE1/AE3) staining (40x). Grouped images are shown at identical magnification.

a

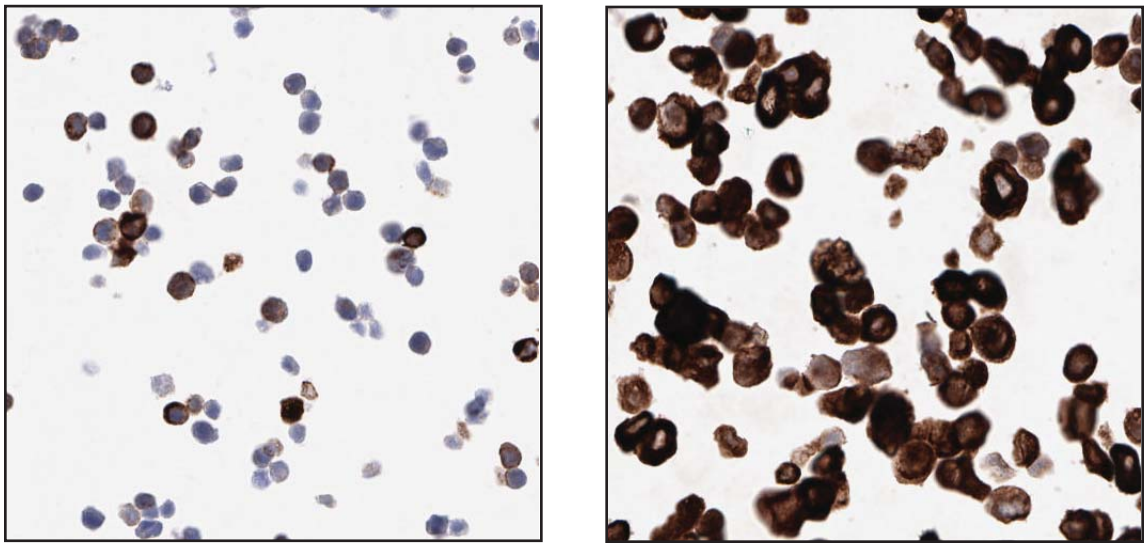

Vehicle JQ1

b

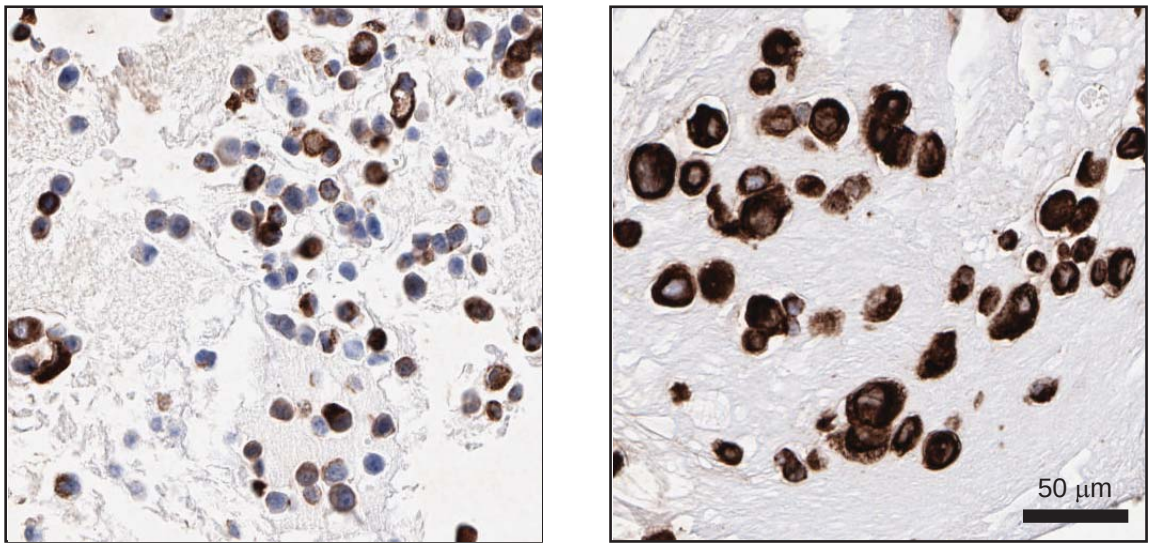

Control BRD4-NUT Knockdown

Supplementary Figure 5 | Squamous differentiation induced by JQ1 is comparable to differentiation induced by RNA silencing of the BRD4-NUT oncoprotein. a, NMC 797 cells were treated with JQ1 (500 nM, 48h) or vehicle control, as shown. Cells were centrifuged, fixed, sectioned and stained for keratin expression (AE1/AE3, 20x). b, NMC 797 cells were transfected with siRNA oligonucleotides directed at the BRD4-NUT transcript (right) or a scrambled control (left). Cells were centrifuged, fixed, sectioned and stained for keratin expression (AE1/AE3, 20x). JQ1 prompts a comparable degree of keratin expression as RNA silencing of the causative oncoprotein in NMC cells.

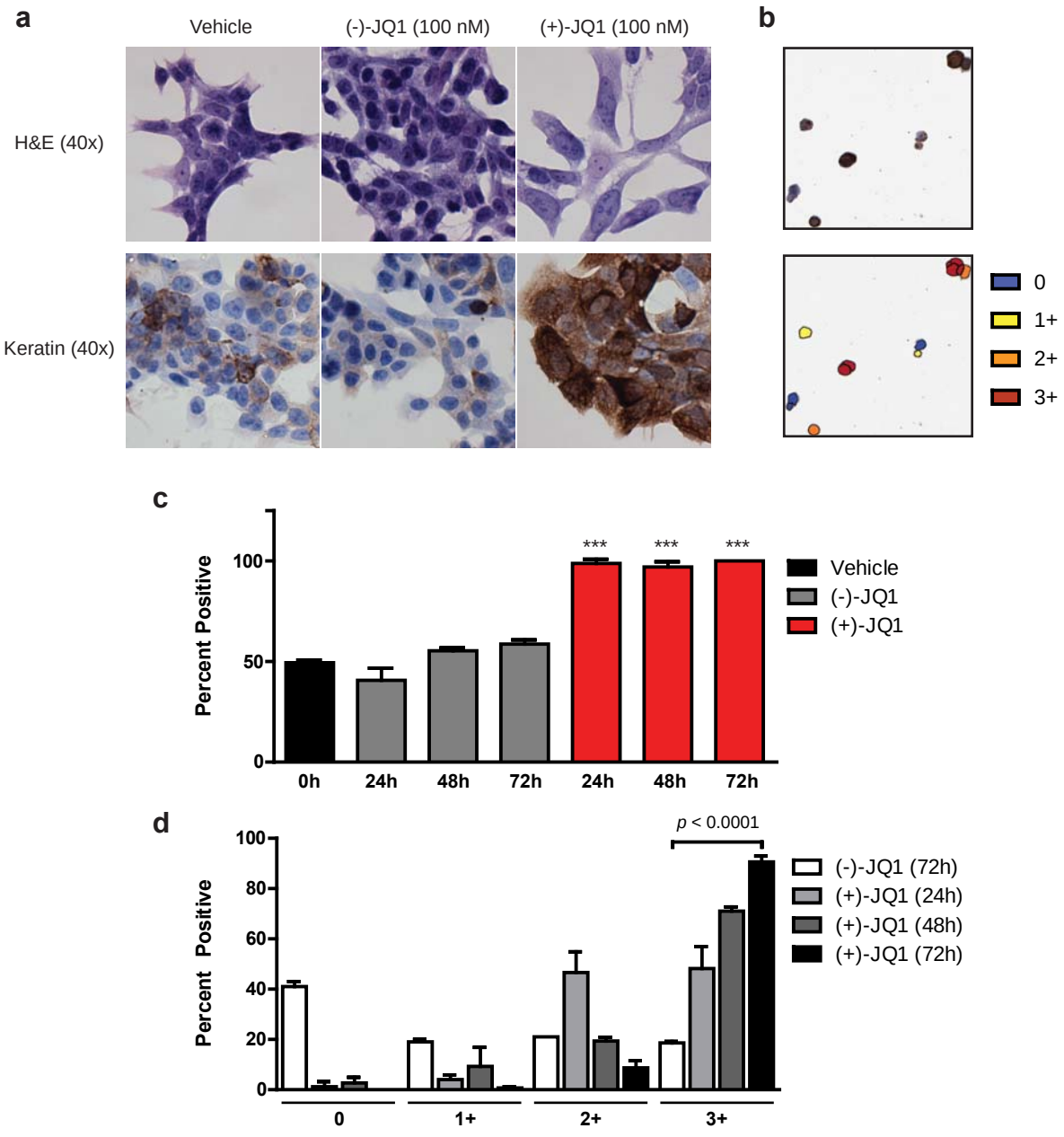

Supplementary Figure 6 | Induction of squamous differentiation in NUT midline carcinoma cells by JQ1 is stereospecific and time-dependent. a, NMC 797 cells treated in chamber slides with (-)-JQ1 (100 nM) exhibit comparable cytosolic phenotypes compared to vehicle-treated controls. (+)-JQ1 (100 nM, 48 h) prompts squamous differentiation exhibited by cell spindling, flattening and increased expression of keratin. b, NMC 797 cells treated with JQ1 enantiomers or vehicle were centrifuged, fixed, sectioned and stained for keratin expression (left; AE1/AE3, 20x). Image-based analysis of keratin expression was performed on concurrently prepared slides using unbiased masking and quantification algorithms capable of scoring nuclei for staining intensity (right; 20x). c, (+)-JQ1 (250 nM) induces rapid expression of keratin in treated NMC 797 cells compared to (-)-JQ1 (250 nM) and vehicle controls, as determined by quantitative immunohistochemistry. Percent positive nuclei per treatment condition are presented. Data represent the mean ± s.d. (n = 3) and are annotated with p-values as obtained from a two-tailed t-test. d, (+)-JQ1 (250 nM) elicits a time-dependent induction of strong (3+) keratin staining of treated NMC 797 cells, compared to (-)-JQ1 (250 nM). Percent positive nuclei per treatment condition are presented. Data represent the mean ± s.d. (n = 3) and are annotated with p-values as obtained from a two-tailed t-test. Grouped images are shown at identical magnification.

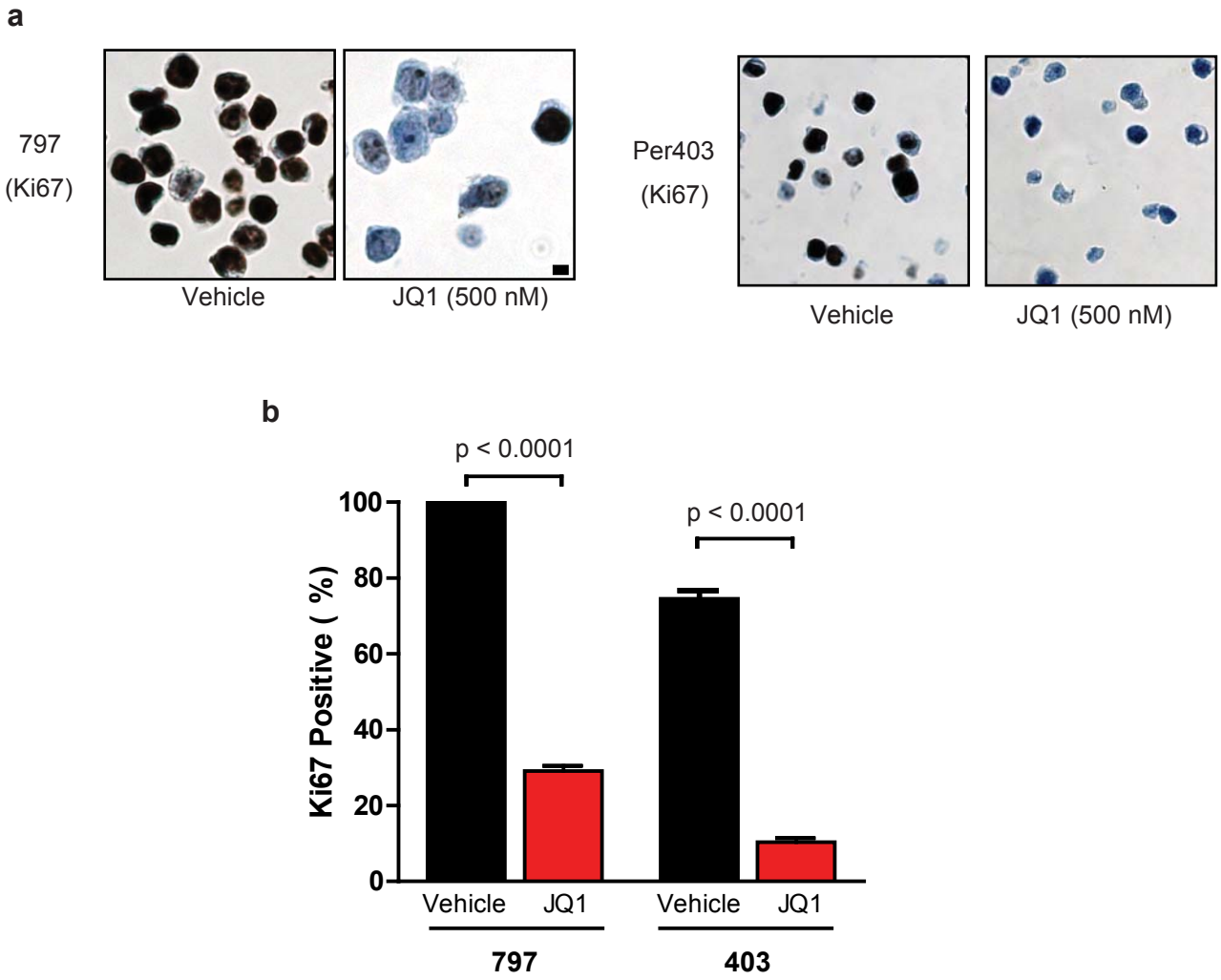

Supplementary Figure 7 | JQ1 impairs NMC cellular proliferation. a, JQ1 attenuates rapid proliferation of NMC 797 and Per403 cell lines in vitro (Ki67; 40x; scale bar is 10 μm). Images are shown at identical magnification. b, Effect of JQ1 on cellular proliferation (Ki67 staining and positivity; %) as measured by IHC as carried out in (a) and Figure 4j. Cells were manually scored as Ki67 positive (dark staining nuclei) or negative (pale blue staining nuclei) in five high-powered fields. Data represent the mean ± s.d. (n = 5), and are annotated with p-values as obtained from a two-tailed t-test.

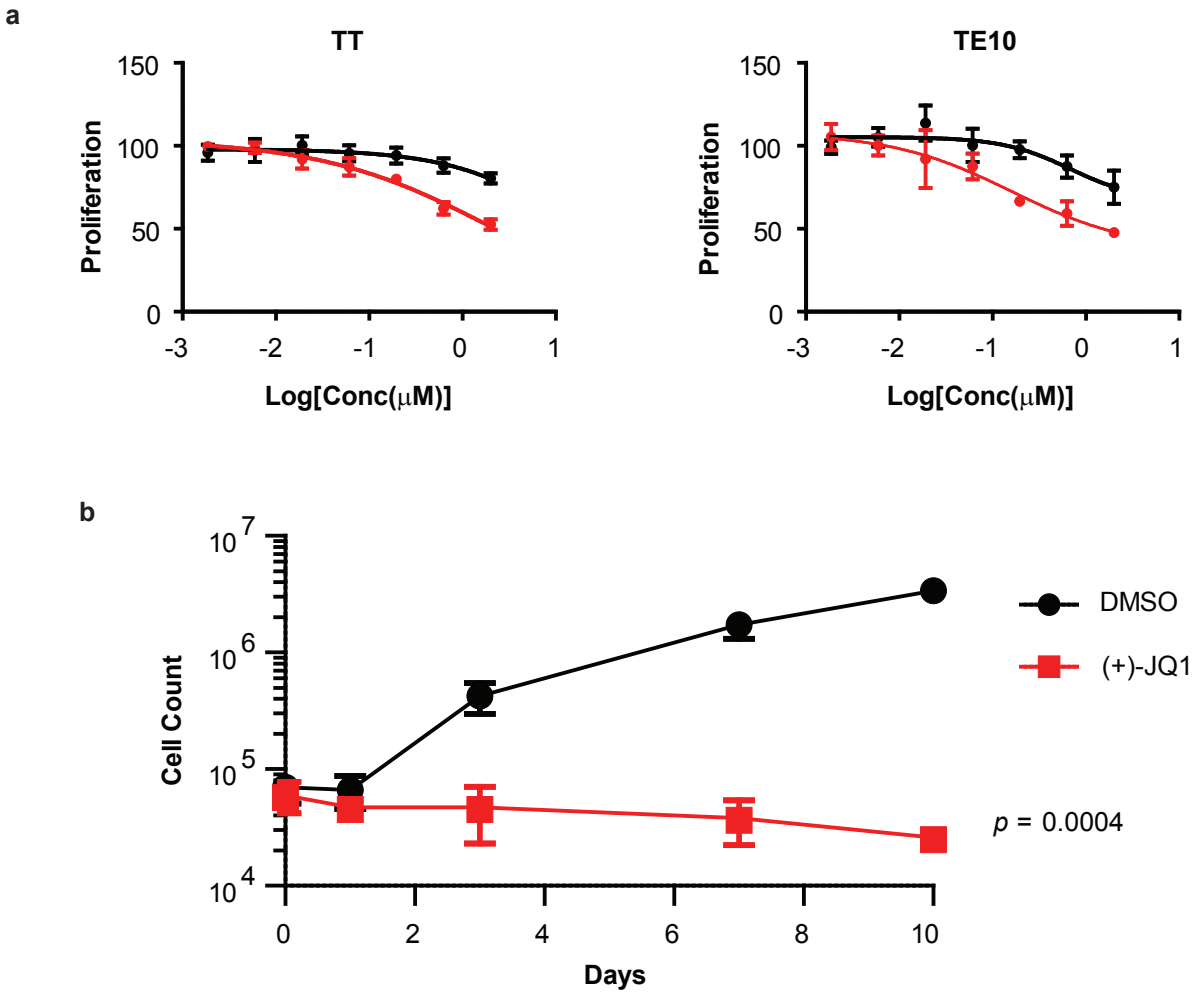

Supplementary Figure 8 | Squamous carcinoma cell lines which do not possess the BRD4-NUT translocation are less sensitive to treatment with JQ1. a, Gastrointestinal squamous carcinoma cell lines (TT and TE10) were cultured in the presence of (+)-JQ1 (250 nM, red circles) or (-)-JQ1 (250 nM, black circles) for 72 hours. Minimal effects observed on cell proliferation with JQ1 is consistent with a plausible role in cell cycle progression in mitotic cells. Data is presented as mean ± s.d. (n = 3). IC50 values were calculated by logistic regression. b, Progressive antiproliferative effects of (+)-JQ1 on NMC 797 cells over time were demonstrated on days 1, 3, 7 and 10. Data points are mean ± s.d. (n = 3).

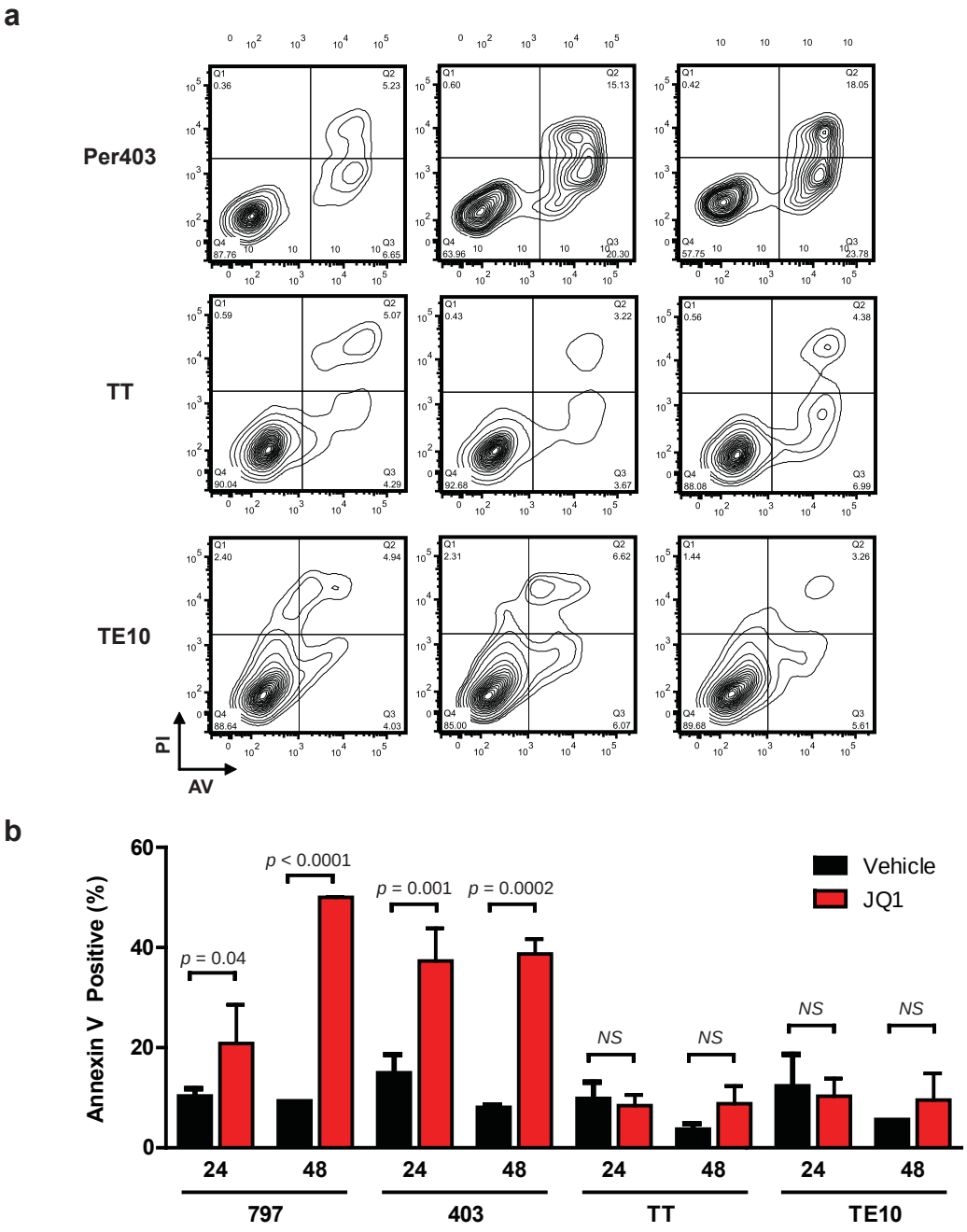

Supplementary Figure 9 | JQ1 selectively induces apoptosis in NMC among human squamous carcinoma cell lines. a, NMC Per403 cells treated with JQ1 (500 nM, 24 or 48 h) exhibit induction of apoptosis by flow cytometry, in contrast to non-NMC squamous carcinoma cell lines TE10 and TT. PI, propidium iodide, AV, annexin V. b, Quantification and comparison of annexin-V positive cells by flow cytometry as performed in (a) and Figure 5d (raw data for NMC 797 cells treated for 24 hours are not shown). JQ1 (500 nM) exhibits a prompt and time-dependent induction of apoptosis in NMC cell lines compared to non-NMC squamous carcinoma cell lines. Data represent the mean ± s.d. (n = 3), and are annotated with p-values as obtained from a two-tailed t-test or NS for non-significant differences.

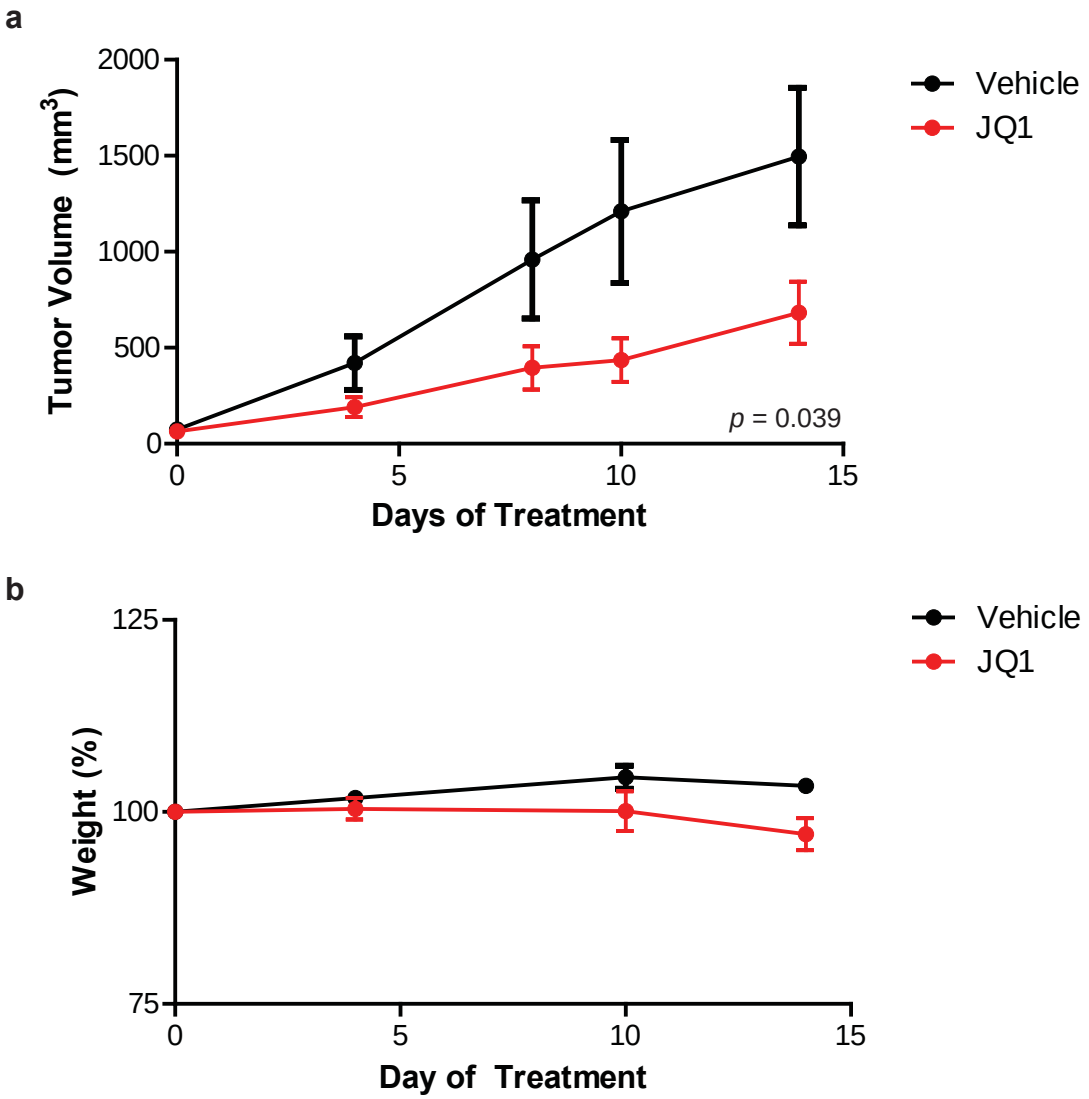

Supplementary Figure 10 | Mice bearing NMC 797 xenografts tolerate JQ1 therapy, which elicits and anti-tumor effect. a, Treatment of NMC 797 xenograft-bearing mice with JQ1 (50 mg kg -1 per day) reduces tumor burden over 14 days of therapy. Data represent the mean ± s.d. (n = 7). b, JQ1 does not produce adverse symptoms or weight loss. Data represent the mean ± s.d. (n = 7).

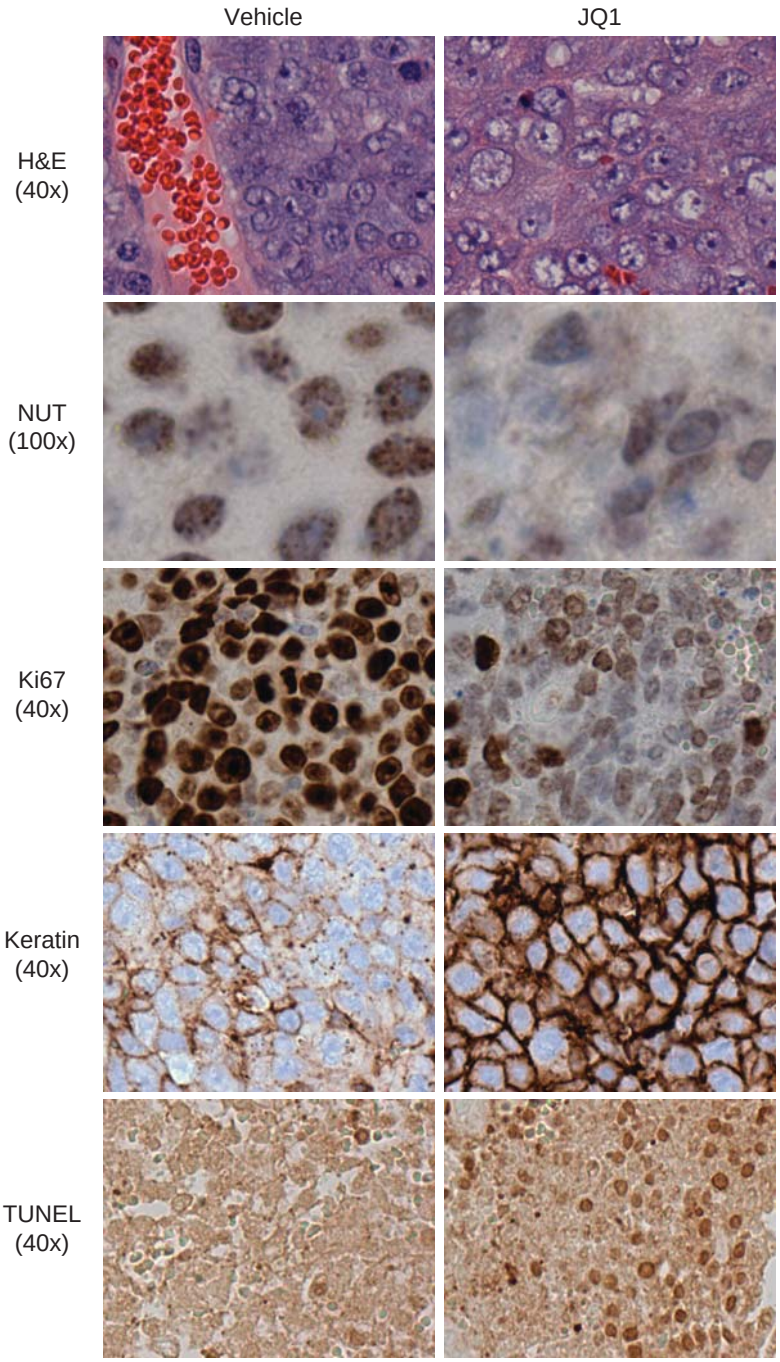

Supplementary Figure 11 | JQ1 prompts squamous differentiation, growth arrest and apoptosis in vivo, as determined by IHC. Histopathological analysis of NMC 797 tumors excised from animals treated with JQ1 (right panel) reveals squamous differentiation (H&E, 40x), effacement of nuclear NUT foci (NUT, 100x), impaired proliferation (Ki67, 40x), induction of keratin expression (AE1/AE3, 40x) and an apoptotic response (TUNEL, 40x), all as compared to vehicle-treated animals (left panel).

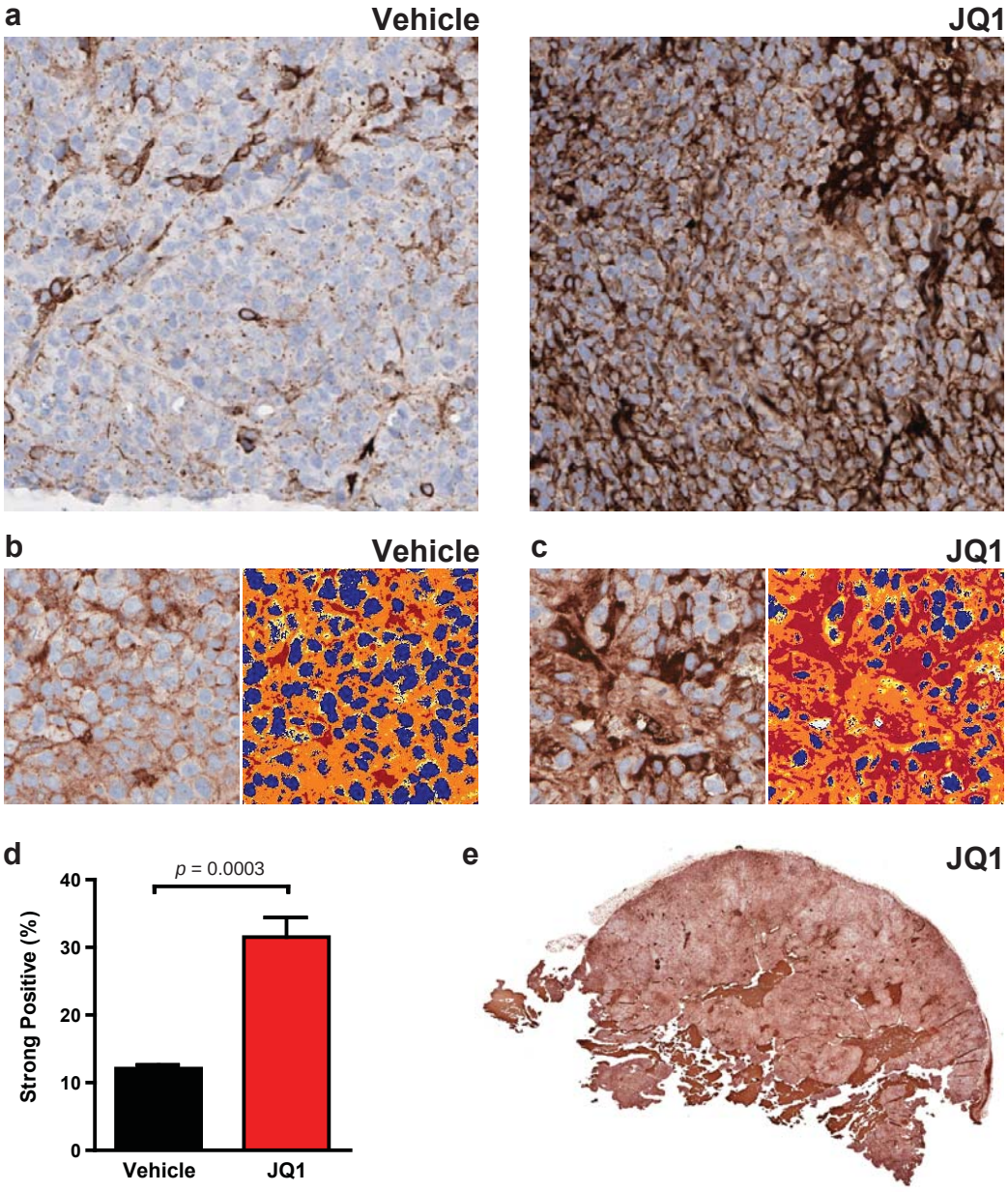

Supplementary Figure 12 | Quantification of diffuse, strong keratin expression induced by JQ1 in NMC 797 xenograft tumors. a, Expanded images of NMC 797 tumors excised from animals treated with JQ1 (50 mg kg -1 per day) or vehicle control are provided. Histopathological analysis of NMC 797 tumors excised from animals treated with JQ1 reveals increased keratin expression (AE1/AE3, 40x) as compared to treatment with vehicle. b, Image-based analysis of keratin expression was performed on stained NMC 797 tumors (left; 20x) derived from vehicle-treated animals using unbiased masking and quantification algorithms capable of scoring individual pixels for staining intensity (right; 20x). c, Image-based analysis of keratin expression was performed on stained NMC 797 tumors (left; 20x) derived from JQ1-treated animals using unbiased masking and quantification algorithms capable of scoring individual pixels for staining intensity (right; 20x). d, JQ1 treatment causes significantly increased expression of keratin (AE1/AE3) in NMC 797 xenografts compared to tumors derived from vehicle-treated animals. Data represent the mean ± s.d. of three independent fields of stained cells within excised tumors. Data are annotated with p-values as obtained from a two-tailed t-test. e, Low magnification (0.8x) image of an excised NMC 797 tumor xenograft sectioned and stained for keratin expression (AE1/AE3). Diffuse staining consistent with a uniform effect on keratin induction in JQ1-treated tumors is observed. All paired images are shown at identical magnification.

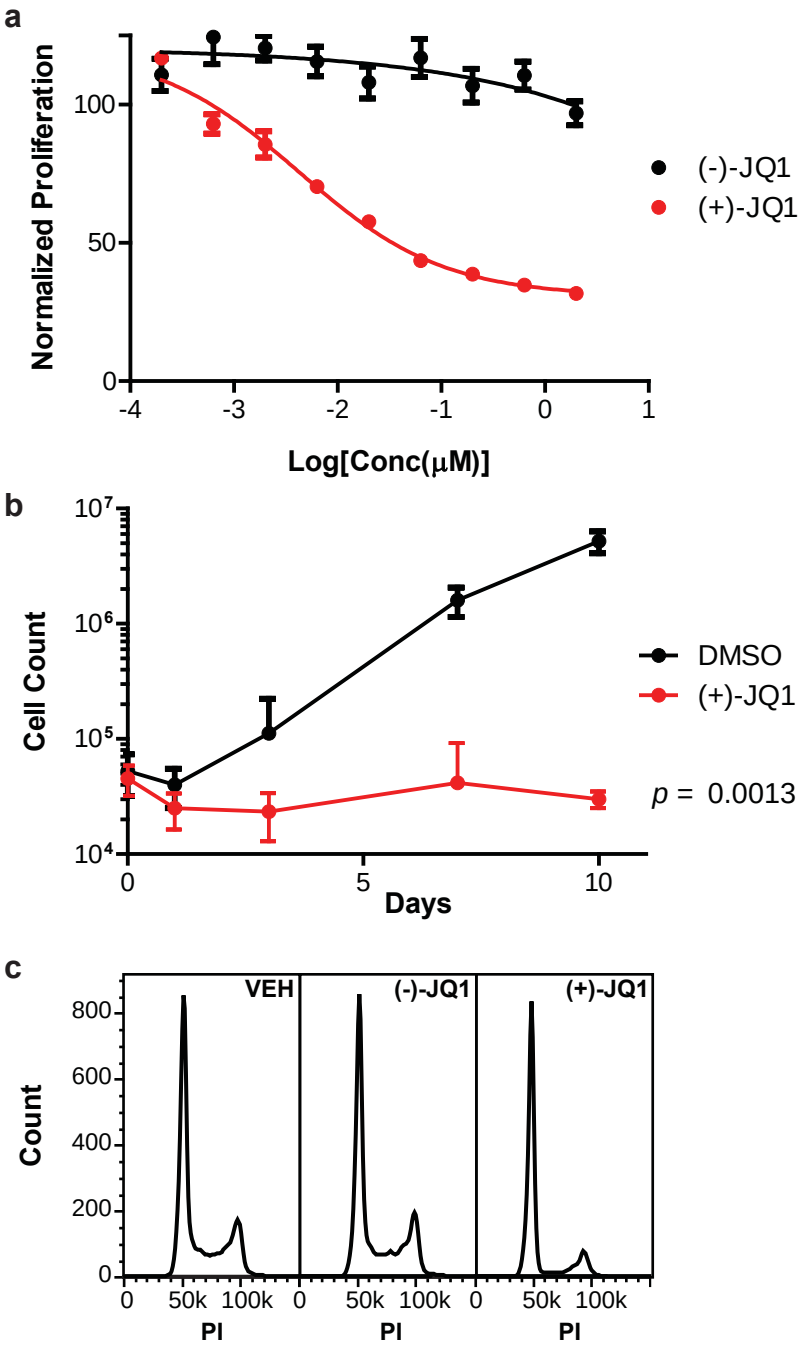

Supplementary Figure 13 | NMC patient-derived tissue is sensitive to the antiproliferative effects of (+)-JQ1 in vitro. a, Patient-derived NMC 11060 cells were isolated from discarded clinical material and grown in short-term cultures for in vitro studies. Antiproliferative effects of BRD4 inhibition on NMC 11060 cells were measured after 72 hours of incubation with (+)-JQ1 (red circles) or (-)-JQ1 (black circles). NMC 11060 cells are uniquely sensitive to the (+)-JQ1 enantiomer. Data is presented as mean ± s.d. (n = 3). IC50 values were calculated by logistic regression. b, Progressive antiproliferative effects of (+)-JQ1 on patient-derived NMC 11060 cells over time as demonstrated on days 1, 3, 7 and 10. Data points are mean ± s.d. (n = 3). c, Flow cytometry for DNA content in NMC 11060 cells. (+)-JQ1 (250 nM, 48 h) induces a G1 arrest compared to (-)-JQ1 (250 nM) and vehicle control.

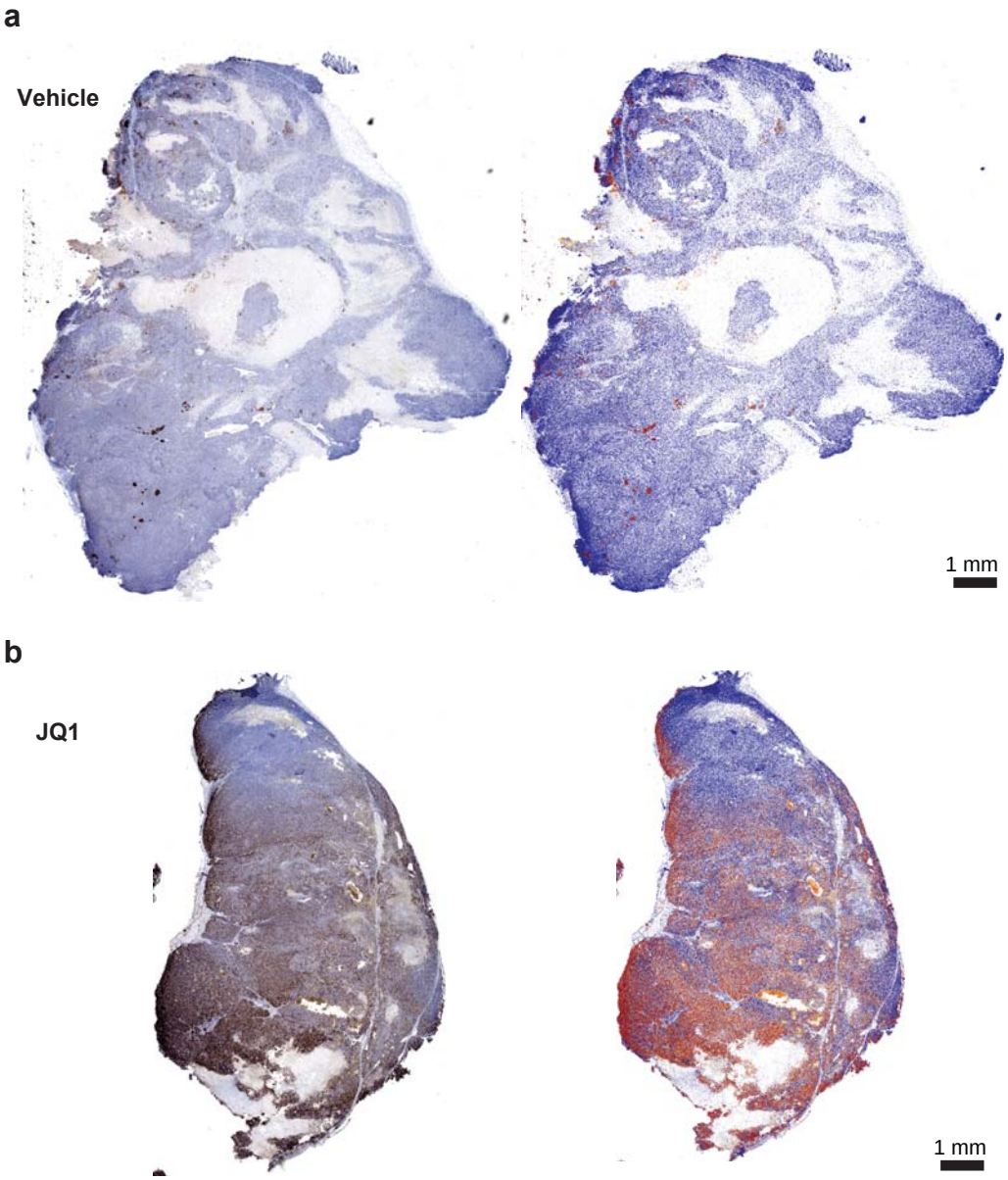

Supplementary Figure 14 | Quantification of diffuse, strong keratin expression induced by JQ1 in patient-derived NMC 11060 primary xenograft tumors. a, Low magnification (0.8x) image of an excised NMC 11060 primary xenograft derived from a vehicle-treated animal, sectioned and stained for keratin expression (AE1/AE3; left). Overall staining for keratin is low throughout the sectioned tumor. Image-based analysis of keratin expression was performed using unbiased masking and quantification algorithms capable of scoring individual pixels for staining intensity (right). b, Low magnification (0.8x) image of an excised NMC 11060 primary xenograft derived from a (+)-JQ1-treated animal (50 mg kg -1 daily for four days), sectioned and stained for keratin expression (AE1/AE3; left). Diffuse staining consistent with a uniform effect on keratin induction in JQ1-treated tumors is observed. Image-based analysis of keratin expression was performed using unbiased masking and quantification algorithms capable of scoring individual pixels for staining intensity (right). Pixel positivity is scored quantitatively and reported visually as blue (0), yellow (1+), orange (2+) and red (3+). All paired images are shown at identical magnification.

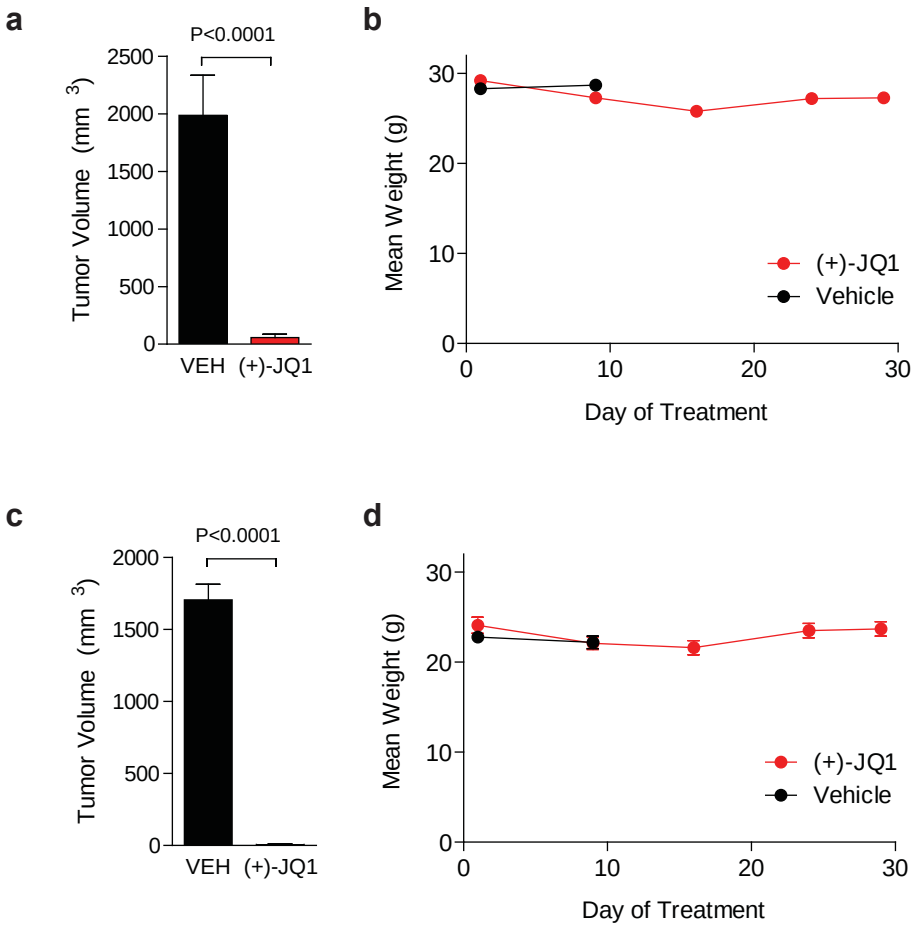

Supplementary Figure 15 | Response of NMC xenografts to (+)-JQ1 and tolerability of daily administration. a, Treatment of NMC 11060 xenograft-bearing mice with (+)-JQ1 (50 mg kg -1 per day) reduces tumor burden after 10 days of therapy (p-values are derived from a two-tailed t-test). Data represent the mean ± s.d. (n = 10). b, JQ1 does not produce adverse symptoms or weight loss through 18 days of therapy. Data represent the mean ± s.d. (n = 10). c, Treatment of NMC Per403 xenograft-bearing mice with (+)-JQ1 (50 mg kg -1 per day) reduces tumor burden after 10 days of therapy (p-values are derived from a two-tailed t-test). Data represent the mean ± s.d. (n = 10). b, JQ1 does not produce adverse symptoms or weight loss through 18 days of therapy. Data represent the mean ± s.d. (n = 10).

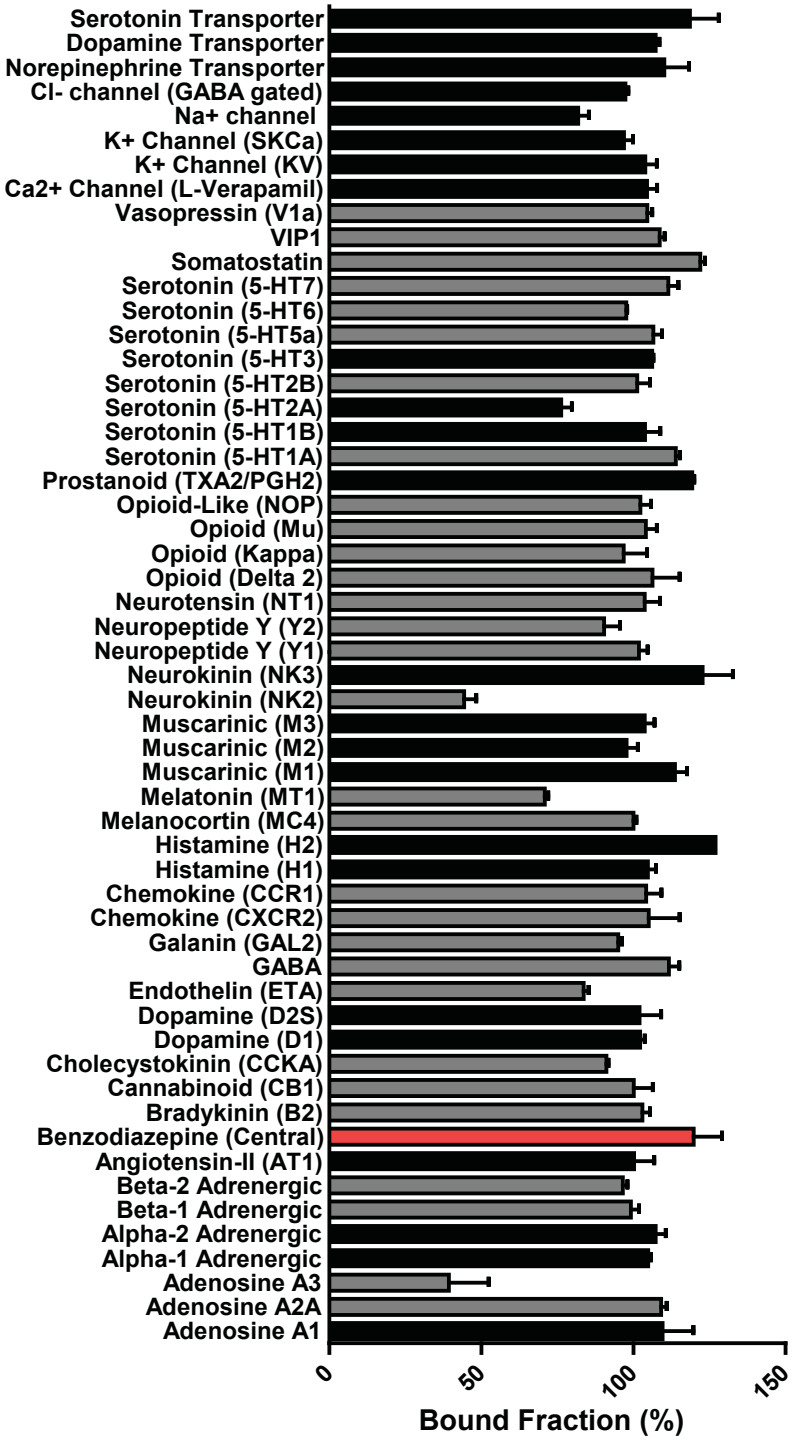

Supplementary Figure 16 | JQ1 exhibits limited activity against a panel of human recombinant ligand and ion receptors. JQ1 (1 μm) was screened against a panel of 55 ligand receptors, ion channels and transport proteins using an established and widely utilized commercial assay (ExpresSProfile; CEREP, Paris, FRANCE). JQ1 exhibited no inhibitory activity toward agonists (gray bars) or antagonists (black bars) binding to 53 receptor proteins, notably including binding of diazepam to the central benzodiazepine receptor (red bar). Data represent mean and SEM of at least three independent measurements. Partial inhibition of binding was observed for the [Nleu-10]-NKA agonist radioligand to the neurokinin NK2 receptor and the agonist IB-MECA [1-Deoxy-1-[6-[[(3-iodophenyl)methyl]amino]-9H-purin-9-yl]-N-methyl-b-D-ribofuranuronamide] to the adenosine A3 receptor. Complete data are provided in Supplementary Table 5.

a

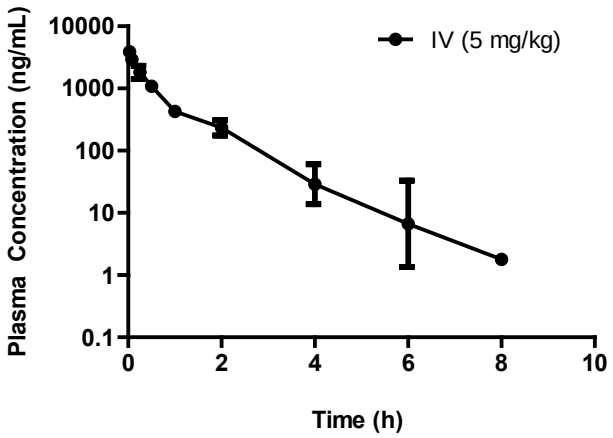

b

PK Parameter	Unit	Estimate
CL	L/hr/kg	2.35
V_{ss}	L/kg	2.02
$T_{1/2}$	hr	0.897
AUC_{last}	hr*ng/mL	2130
AUC_{INF}	hr*ng/mL	2130
MRT_{INF}	hr	0.861

c

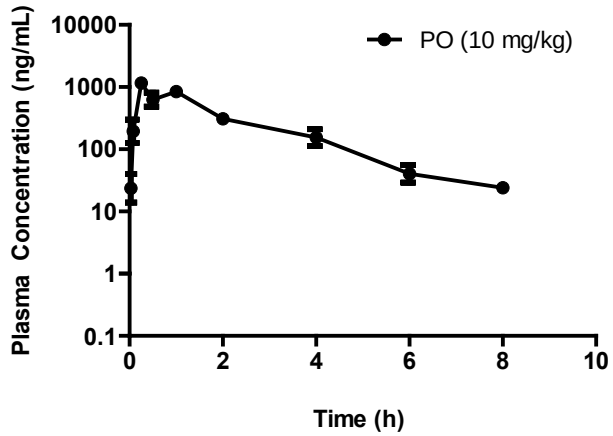

d

PK Parameter	Unit	Estimate
T_{max}	hr	0.250
C_{max}	ng/mL	1180
$T_{1/2}$	hr	1.39
AUC_{last}	hr*ng/mL	2040
AUC_{INF}	hr*ng/mL	2090
F	%	49.1

Supplementary Figure 17 | JQ1 exhibits excellent oral bioavailability and adequate pharmacokinetic exposure in rodents. Pharmacokinetic studies of (+)-JQ1 were performed in CD1 mice following intravenous (a, b) and oral (b, c) administration. a, Mean plasma concentration-time profiles of (+)-JQ1 after intravenous dosing (5 mg kg -1). Data represent the mean and s.d. (n = 3). b, Calculated pharmacokinetic parameters for intravenous (+)-JQ1 demonstrate excellent drug exposure [Area under the curve (AUC) = 2090 hr*ng/mL] and an approximately one hour half-life (T1/2). c, Mean plasma concentration-time profiles of (+)-JQ1 after oral dosing (10 mg kg -1). Data represent the mean and s.d. (n = 3). d, Calculated pharmacokinetic parameters for oral (+)-JQ1 demonstrate excellent oral bioavailability (F = 49%), peak plasma concentration (Cmax = 1180 ng/mL) and drug exposure (AUC = 2090 hr*ng/mL). CL, clearance; Vss, volume in steady-state; MRTINF, mean residence time extrapolated to infinity; Tmax, time to maximum concentration.

Methods

Reagents. Endogenous BRD4-NUT-expressing midline carcinoma cell lines, 797[44] and PER-403[45], were described previously. The non-NMC human squamous carcinoma cell lines TE10 and TT were obtained from Drs. Anil Rustgi (University of Pennsylvania) and Adam Bass (Dana-Farber Cancer Institute). U2OS cells were obtained from the ATCC. Mammalian overexpression constructs for GFP-BRD4, GFP-NUT and GFP-BRD4-NUT have been previously described[46]. Media, trypsin, and antibiotics for tissue culture were purchased from Mediatech. Antibodies and stains for immunohistochemistry and flow cytometry were obtained from Dako (Cytokeratin AE1/AE3 antibody Cat# N1590), Millipore (TUNEL Cat# S7100), Vector (Ki67 Cat# VP-RM04), Cell Signaling Technologies (NUT Cat# 3625), BD Pharmingen (Annexin V-FITC Cat# 556547) and Invitrogen (propidium iodide Cat# P3566).

Cloning. cDNA encoding human BRD2, BRD3, BRD4, BRDT, CREBBP and WDR9 (NCBI accession number NP 005095, NP 031397.1, NP 055114.1, NP 001717.2, NP 004371.1, NP 061836.2) were obtained from different sources (BRD2: Synthetic, BRD3: Origene, BRD4: FivePrime, BRDT: IMAGE collection, CREBBP: Synthetic, WDR9: synthetic) and used as templates to amplify the bromodomain regions of the above proteins, using the polymerase chain reaction (PCR) in the presence of Platinum® Pfx DNA polymerase (Invitrogen™, UK). PCR products were purified (QIAquick PCR Purification Kit, Qiagen Ltd. UK) and further sub-cloned into a pET28 derived expression vector, pNIC28-Bsa4[47], using ligation independent cloning[48]. The constructs were transformed into competent Mach1™ cells (Invitrogen™, UK) to yield the final plasmid DNA.

Protein Expression and Purification. Colonies from freshly transformed plasmid DNA in competent *E. coli* BL21(DE3)-R3-pRARE2 cells (phage-resistant derivative of

BL21(DE3) strain), with a pRARE plasmid encoding rare codon tRNAs were grown overnight at 37 ºC in 5 ml of Luria-Bertani medium (LB-broth, Merck) with 50 µg/ml kanamycin and 34 µg/ml chloramphenicol (start-up culture). The start-up culture was diluted 1:1000 in fresh medium and cell growth was allowed at 37 ºC to an optical density of about 0.5 (OD600) before the temperature was decreased to 18 ºC. When the system equilibrated at 18 ºC the optical density was about 0.8 (OD600) and protein expression was induced over night at 18 ºC with 0.1 mM isopropyl-β-D-thiogalactopyranoside (IPTG). The bacteria were harvested by centrifugation (8,700 x g for 15 min at 4 ºC, JLA 81,000 rotor, on a Beckman Coulter Avanti J-20 XP centrifuge) and were frozen at -20 ºC as pellets for storage. Cells expressing His6-tagged proteins were re-suspended in lysis buffer (50 mM HEPES, pH 7.5 at 25 ºC, 500 mM NaCl, 5 mM Imidazole, 5 % glycerol and 0.5 mM TCEP (Tris(2-carboxyethyl)phosphine hydrochloride)) in the presence of protease inhibitor cocktail (1 µl/ml) and lysed using an EmulsiFlex-C5 high pressure homogenizer (Avestin - Mannheim, Germany) at 4 ºC. 0.15 % of PEI (polyethyleneimine) was added for 30 min on ice and the lysate was cleared by centrifugation (16,000 x g for 1 h at 4 ºC, JA 25.50 rotor, on a Beckman Coulter Avanti J-20 XP centrifuge) and was applied to a nickel-nitrilotiacetic acid agarose column (Ni-NTA, Qiagen Ltd., 5 ml, equilibrated with 20 ml lysis buffer). The column was washed once with 30 ml of lysis buffer then twice with 10 ml of lysis buffer containing 30 mM Imidazole. The protein was eluted using a step elution of Imidazole in lysis buffer (50, 100, 150, 2 x 250 mM Imidazole in 50 mM HEPES, pH 7.5 at 25 ºC, 500 mM NaCl). All fractions were collected and monitored by SDS-polyacrylamide gel electrophoresis (Bio-Rad Criterion™ Precast Gels, 4-12 % Bis-Tris, 1.0 mm, from Bio-Rad, CA.). After the addition of 10 mM dithiothreitol (DTT), the eluted protein was treated overnight at 4 ºC with Tobacco Etch Virus (TEV) protease to remove the hexa-histidine tag. The protein was further purified with size exclusion chromatography on a Superdex 75 16/60 HiLoad gel filtration column (GE/Amersham Biosciences) on an ÄktaPrime™ plus system

(GE/Amersham Biosciences). Samples were monitored by SDS-polyacrylamide gel electrophoresis and concentrated to 10-40 mg/ml in the gel filtration buffer, 10 mM Hepes pH 7.5, 150 mM NaCl, 0.5 mM TCEP and were used for crystallization. Samples for isothermal calorimetry were dialysed over night at 4 ºC in a D-Tube™ Dialyser Midi, MWCO 3.5 kDa to a final buffer of 50 mM HEPES, pH 7.4 (at 25 ºC), 150 mM NaCl. Protein handling was carried out on ice or in a cold room in all the above steps.

Electro-spray Mass Spectrometry (ESI-TOF). Concentrated protein samples were diluted at 1 mg/ml in 0.1 % formic acid and 30 µl were injected on an Agilent 1100 Series LC/MSD TOF (Agilent Technologies Inc. - Palo Alto, CA) mass spectrometer with a Zorbax 5 µm 300SB-C3 column (Agilent Technologies Inc. - Palo Alto, CA) in order to ascertain the correct mass of the protein constructs (14.897 kDa for BRD2(1), 15.4316 kDa for BRD2(2), 14.570 kDa for BRD3(1), 13.284 kDa for BRD3(2), 15.084 kDa for BRD4(1), 15.036 kDa for BRD4(2), 14.149 kDa for BRDT(1), 14.207 kDa for CREBBP and 14.429 kDa for WDR9(2)). Raw ion count data were deconvoluted using the software package Proteins (version A.01.00, Agilent Technologies Inc. - Palo Alto, CA), or MAGTRAN[49] (version 1.02). The corrected mass and purity was confirmed for all recombinant proteins.

Protein stability shift assay. Thermal melting experiments were carried out using an Mx3005p Real Time PCR machine (Stratagene). Proteins were buffered in 10 mM HEPES pH 7.5, 500 mM NaCl and assayed in a 96-well plate at a final concentration of 2 µM in 20 µl volume. Compounds were added at a final concentration of 10 µM. SYPRO Orange (Molecular Probes) was added as a fluorescence probe at a dilution of 1:1000. Excitation and emission filters for the SYPRO-Orange dye were set to 465 nm and 590 nm, respectively. The temperature was raised with a step of 3 °C per minute from 25 ºC to 96 ºC and fluorescence readings were taken at each interval. The temperature

dependence of the fluorescence during the protein denaturation process was approximated by the equation

$$y(T) = y_F + \frac{y_U - y_F}{1 + e^{\Delta uG_{(T)}/RT}}$$

where $\Delta uG_{(T)}$ is the difference in unfolding free energy between the folded and unfolded state, R is the gas constant and y_F and y_U are the fluorescence intensity of the probe in the presence of completely folded and unfolded protein respectively. The baselines of the denatured and native states were approximated by a linear fit. The observed temperature shifts, ΔT_m^{obs}, were recorded as the difference between the transition midpoints of sample and reference wells containing protein without ligand in the same plate and determined by non-linear least squares fit.

Isothermal Titration Calorimetry. Experiments were carried out on a VP-ITC titration microcalorimeter from MicroCal™, LLC (Northampton, MA). All experiments were carried out at 15 ºC while stirring at 295 rpm, in ITC buffer (50 mM HEPES pH 7.4 at 25 ºC, 150 mM NaCl). The microsyringe (250 µl) was loaded with a solution of the protein sample (300 µM protein for the BETs, 950 µM protein for CREBBP and 600 µM for WDR9(2), in ITC buffer). All titrations were conducted using an initial injection of 2 µl followed by 34 identical injections of 8 µl with a duration of 16 sec (per injection) and a spacing of 250 sec between injections. The heat of dilution was determined by independent titrations (protein into buffer) and was subtracted from the experimental data. The collected data were implicated in the MicroCal™ Origin software supplied with the instrument to yield enthalpies of binding (ΔH) and binding constants (K_B) as previously described by Wiseman and coworkers[50]. Thermodynamic parameters were calculated ($\Delta G = \Delta H - T\Delta S = -RT\ln K_B$, where ΔG, ΔH and ΔS are the changes in free energy, enthalpy and entropy of binding respectively). In all cases a single binding site

model was employed. Dissociation constants and thermodynamic parameters are listed in Supplementary Table 3.

Acetyl-Histone Binding Assay. Assays were performed as described previously[51] with minor modifications from the manufacturer's protocol (PerkinElmer, USA). All reagents were diluted in 50 mM HEPES, 100 mM NaCl, 0.1 % BSA, pH 7.4 supplemented with 0.05 % CHAPS and allowed to equilibrate to room temperature prior to addition to plates. A 24-point 1:2 serial dilution of the ligands was prepared over the range of 150 – 0 μM and 4 μl transferred to low-volume 384-well plates (ProxiPlateTM-384 Plus, PerkinElmer, USA), followed by 4 μl of His-tagged protein (BRD4(1), 250 nM, BRD4(2) and CREBBP, 2000 nM). Plates were sealed and incubated at room temperature for 30 minutes, before the addition of 4 μl of biotinylated peptide at equimolar concentration to the protein [peptide for BRD4(1) & BRD4(2): H4K5acK8acK12acK16ac, H-SGRGK(Ac)GGK(Ac)GLGK(Ac)GGAK(Ac)RHRK(Biotin)-OH; peptide for CREBBP: H3K36ac, Biotin-KSAPATGGVK(Ac)KPHRYRPGT-OH (Cambridge Research Biochemicals, UK)]. Plates were sealed and incubated for a further 30 minutes, before the addition of 4 μl of streptavidin-coated donor beads (25 μg/ml) and 4 μl nickel chelate acceptor beads (25 μg/ml) under low light conditions. Plates were foil-sealed to protect from light, incubated at room temperature for 60 minutes and read on a PHERAstar FS plate reader (BMG Labtech, Germany) using an AlphaScreen 680 excitation/570 emission filter set. IC_{50} values were calculated in Prism 5 (GraphPad Software, USA) after normalization against corresponding DMSO controls and are given as the final concentration of compound in the 20 μl reaction volume.

Crystallization. Aliquots of the purified proteins were set up for crystallization using the vapour diffusion method and a mosquito® crystallization robot (TTP Labtech, Royston UK). Coarse screens were typically setup onto Greiner or SWISSCI 3-well plates using three different drop ratios of precipitant to protein per condition (100 + 50 nl, 75 + 75 nl

and 50 + 100 nl). Initial hits were optimized further using 1 or 3-well plates and scaling up the drop sizes in steps. All crystallizations were carried out using sitting drops at 4 ºC. BRD2(2) crystals in complex with **JQ1** (I) were grown by mixing 150 nl of protein (11.2 mg/ml) with an equal amount of reservoir solution containing 30 % jeffamine 600, 0.05 M CsCl and 0.1 M MES pH 6.5. BRD4(1) crystals (II) were grown by mixing 75 nl of the protein (9 mg/ml) with an equal volume of reservoir solution containing 0.2 M $NaNO_3$, 20 % polyethylene glycol PEG3350 and 10 % ethylene glycol. Its complex with **JQ1** (III) was grown by mixing 150 nl of the protein (10.1 mg/ml) with 150 nl of reservoir solution containing 0.2 M NaI, 0.1 M Bis-Tris-Propane pH 8.5, 20 % PEG 3350 and 10 % ethylene glycol. Crystals grew to diffracting quality within 1-3 weeks in all cases.

Data Collection and Structure Solution. Crystals were cryo-protected using the well solution supplemented with 25 % additional ethylene glycol in the case of II and III and were flash frozen in liquid nitrogen or were flash frozen without any additional cryoprotection in the case of I. Data were collected at a Rigaku FRE rotating anode, equipped with Osmic HR optics and a Rigaku HTC image plate detector at 1.542 Å (I, III) or at the Swiss Light Source on beamline X10SA using a MAR225 detector at 1.0023 Å (II). Indexing integration and scaling was carried out using MOSFLM[52] and SCALA[53] (I, III) or HKL2000[54] (II). Initial phases were calculated for (II) by molecular replacement with PHASER[55] using an ensemble of known human bromodomains (PBD IDs 2NXB, 2OO1). Phases for I and III were calculated using the model of II. Initial models were built by ARP/wARP[56] and building was completed manually with COOT[57]. Refinement was carried out in REFMAC5[58]. In all cases thermal motions were analyzed using TLSMD[59] and hydrogen atoms were included in late refinement cycles. Data collection and refinement statistics can be found in Supplementary Table 4. The models

and structure factors have been deposited with PDB accession codes: 3ONI (I), 2OO1 (II), 3MXF (III).

Docking Studies: Docking studies were performed using the Schrödinger 2007 Suite. The protein structure of BRD4(1) in complex with **(+)-JQ1** was used to build the docking grid. The X-ray structure was pre-processed using the Protein Preparation Module and a 12 Å grid was built around the active site as defined by the position of **(+)-JQ1**. Water molecules beyond 5 Å of the active site were removed. The two stereoisomers of **JQ1** (**(+)-JQ1** and **(-)-JQ1**)) were prepared using the Ligprep module to obtain accurate, energy minimized 3D structures, which were then screened in Glide 4.5, using the extra precision scoring algorithm (XP mode). The top 200 poses were saved and analyzed. Visualizations for structural models were generated using the PyMol molecular visualization package (Schrödinger).

Molecular Dynamics. Molecular dynamics simulations were performed on BRD4(1) alone and in complex with **JQ1** in analogy to our previous studies[60]. In both simulations, the starting coordinates were obtained from the X-ray crystal structures. Solvent molecules beyond 5Å from the active site were removed. The protein preparation panel in Schrödinger 2007 Suite was applied to assign the protonation states and orientations of residues in BRD4(1), which was then further prepared in LEaP module in Amber 10[61], using the ff03 force field. Chloride ions were added to the system for neutralization, followed by solvating the system using TIP3P water box extending 10 Å from the protein. The final system contained 127 protein residues. The protein-ligand complex with **(+)-JQ1** was prepared in the same fashion. The RESP charges of **JQ1** were assigned using the antechamber program in Amber 10, after single point charge calculation at HF/6-31G* level based on the pose of **JQ1** in the X-ray structure. The GAFF force field was used in LEaP to assign the parameters for **JQ1**. In both cases protein minimization, equilibration and molecular dynamics simulations were carried out using the pmemd

module in Amber 10. The temperature was kept at 300 K using Langevin Dynamics. Particle-Mesh-Ewald (PME) summation was applied to treat long-range interactions. The SHAKE algorithm was employed on atoms covalently bound to a hydrogen atom to allow an integration time step of 2 fs. For both systems, 20 ns MD simulations were performed to study the flexibility of BRD4(1) with and without **JQ1**. The energy of both simulations converged and after simulation as shown in Figure 3 of the Supporting Information. Trajectories for both structures were analyzed using the PTRAJ module in Amber 10. Visualizations for structural models were generated using the PyMol molecular visualization package (Schrödinger).

Sequence Alignment. Amino acid sequences for full length human bromodomains were obtained from the NCBI (BRD2 Acession No. NP_005095, BRD3 Acession No. NP_031397.1, BRD4 Acession No. NP_055114.1, BRD-T Acession No. NP_001717.2). Multiple sequence alignment of individual bromodomains was performed using ClustalW[62].

Fluorescence Recovery After Photobleaching (FRAP). FRAP studies were performed on U2OS cells as previously described[46,63]. In brief, U2OS cells were transfected (lipofectamine; Invitrogen) with mammalian overexpression constructs encoding GFP chimera with BRD4, NUT and BRD4-NUT. A 5 μm^2 nuclear region was bleached with high laser intensity in one cell within each field, and measured for recovery with low laser intensity and a 150 μm pinhole. Images of identical fields were acquired using a Nikon C1 Plus confocal microscope equipped with a 37 ºC heated chamber and FRAP modules. Average intensities of the bleached region were measured over time and using MetaMorph v7, and normalized to an independent region of interest before bleaching. Data were then analyzed to assess the time to half-maximal fluorescence recovery and the mobile fraction in Microsoft Excel Mac 12.2.4.

Differentiation and Proliferation Immunohistochemistry. Cultured cancer cell lines (797, Per403, TT and TE10) were grown in chamber slides at 1.0 x 10^4 cells per chamber (4-chamber slides) or 5.0 x 10^3 cells per chamber (8-chamber slides). Cells were treated with **JQ1**-racemic, **(+)-JQ1**, **(-)-JQ1**, or vehicle (DMSO) and incubated for various time intervals. Media was then removed and chambers were washed with cold PBS. Cells were then fixed in 4 % formaldehyde for 20 min at 4 ºC, washed with PBS and transferred to the Dana-Farber/Harvard Cancer Center (DF/HCC) Specialized Histopathology Services Core at Brigham and Women's Hospital for staining, as described below. Immunohistochemical studies of cell pellets were performed by first growing cancer cell lines (797 and Per403) in T-75 flasks, treated with either **JQ1** or vehicle (DMSO) for 48 hours. Cells were then trypsinized and cell pellets were formed by centrifugation at 2,000 rpm for 10 minutes, stabilized with ½ volume of HistoGel (Richard-Allen Scientific) and 10 % bovine serum albumin. Cell pellets were washed with PBS and fixed in 4 % formaldehyde for 20 min at 4 ºC. The cells were then washed with PBS and transferred to the DF/HCC Core Laboratory at the Brigham and Women's Hospital for staining, as described below. Quantitative analysis of Ki67 staining (cell scoring) was performed by light microscopy using five high-powered (40x) fields-of-view per experiment. All fixed material was embedded, sectioned and stained by the DF/HCC Core Laboratory at Brigham and Women's Hospital, using established optimized protocols. Images were obtained using an Olympus BX40 microscope (Olympus Imaging America, Center Valley, PA) and a Micropublisher 3.3 RTV color camera (QImaging, Surrey, BC). Quantitative immunohistochemistry was performed using the Aperio Digital Pathology Environment (Aperio Technologies, Vista, CA) at the DF/HCC Core Laboratory at the Brigham and Women's Hospital. In brief, slides were scanned in an automated fashion on a ScanScope XT Instrument at 20x resolution with the ScanScope Console v10 (Aperio Technologies). Digital images were remotely analyzed using ImageScope (Aperio Technologies). Algorithms for nuclear scoring and

pixel positivity were modified to discriminate degrees of 3,3'-diaminobenzidine staining in paired samples. IHC images and masks were exported as high-resolution TIFF files with comparable settings for paired data. Quantitative data were exported as tab delimited text files for analysis in GraphPad Prism 5.02. Whole-tumor images were exported at 0.8x resolution and prepared for publication using Adobe Photoshop (Adobe Systems, San Jose, CA).

Cell Proliferation Assay. Cells were seeded into white, 384-well microtiter plates (Nunc) at 500 cells per well in a total volume of 50 µl media. The 797, TT and TE10 cells were grown in DMEM containing 1 % penicillin/streptomycin and 10 % FBS. The Per403 cells were grown in DMEM containing 1 % penicillin/streptomycin and 20 % FBS. Patient-derived NMC 11060 cells were grown in RPMI with 10 % FBS and 1% penicillin/streptomycin. Compounds were delivered to microtiter assay plates by robotic pin transfer (PerkinElmer JANUS equipped with a V&P Scientific 100 nl pin tool). Following a 48 h incubation at 37 ºC, cells were lysed and wells were assessed for total ATP content using a commercial proliferation assay (Cell TiterGlo; Promega). Replicate measurements were analyzed with respect to dose and estimates of IC_{50} were calculated by logistic regression (GraphPad Prism).

Cell Growth Assay. Cells were seeded in 6-well tissue culture dishes at a concentration of 1.5 x 10^4 cells per well. Cells were grown in 2 ml of either DMEM (797) or RPMI (11060) containing 10 % fetal bovine serum, 1 % penicillin/streptomycin and either 250 nM **(+)-JQ1** or the equivalent volume of DMSO (0.025 %). One half of the media in each well was replaced daily. On days 0, 1, 3, 7 and 10, dishes of cells assigned to each time point were trypsinized, mixed in a 1:1 ratio with 0.4 % trypan blue and counted using a Countess automated cell counter (Invitrogen).

Flow Cytometry. Cultured human cancer cells (797, Per403, TT and TE10) were grown in 6-well tissue culture plates (BD Falcon) at a starting concentration of 5.0 x 104 cells per well. Cells were treated with **JQ1** (500 nM), staurosporine (50 nM) or vehicle (DMSO 0.05 %) for 24 or 48 h. Trypsinized cells were mixed 1:1 on ice with Annexin-V/propidium iodide buffer (10 mM HEPES pH 7.4, 140 mM NaCl, 2.5 mM $CaCl_2$) containing Annexin V-FITC (BD Pharmingen, 1:500) and propidium iodide (Invitrogen, 1:1000). Samples were immediately analyzed on a BD FACS Canto II. Visualizations and analyses of apoptotic fractions were generated using FlowJo flow cytometry analysis software (Tree Star, Inc.).

Cell Cycle Analysis by Flow Cytometry. NUT midline carcinoma patient cell lines (797 and 11060) were plated in T-25 flasks and grown in DMEM (797) or RPMI (11060) containing 10 % fetal bovine serum and 1 % penicillin/streptomycin. Cells were treated with either 250 nM **(+)-JQ1**, 250 nM **(-)-JQ1** or the equivalent volume of DMSO (0.025 %). At the desired time point, 2 x 10^6 cells were spun at 500 x g for 5 minutes at 4 °C and washed with PBS. Pellets were resuspended in 1 ml of cold PBS and added dropwise while gently vortexing to 9 ml 70 % ethanol in a 15 ml polypropylene centrifuge tube. Fixed cells were then frozen at –20 °C overnight. The next day, cells were centrifuged at 500 x g for 10 minutes at 4 °C and washed with 3 ml of cold PBS. Cells were resuspended in 500 µl of propidium iodide staining solution (0.2 mg/ml RNAse A, 0.02 mg/ml propidium iodide, 0.1 % Triton-X in PBS) and incubated for 20 minutes at 37 °C. Samples were then transferred to ice and analyzed on a BD FACS Canto II. Histograms were generated and cell cycle analysis was performed using FlowJo flow cytometry analysis software (Tree Star, Inc.).

Quantitative RT-PCR Analysis. NMC 797 cells were plated in six-well dishes and treated with vehicle (DMSO), **(+)-JQ1** or **(-)-JQ1** at 250 nM for 48 hours. RNA extraction was performed using TRIzol Reagent (Invitrogen). Superscript II (Invitrogen) was used to prepare cDNA from purified RNA, using oligo dT first-strand synthesis as in the Manufacturer's protocol. Real-time qPCR was performed on an Applied Biosystems 7500 Real-Time PCR system with mammalian Taqman probes from Applied Biosystems [KRT10 (Hs00166289_m1), KRT14 (Hs00265033_m1), TGM1 (Hs00165929_m1), Rad21 (Hs00366726_m1), Ran (Hs00741099_g1), and GAPDH (Hs03929097_g1)] following the Manufacturer's protocol. Analysis was performed on triplicate PCR data per biological replicate. Three biological replicates were used for vehicle (DMSO) and **(-)-JQ1** treated cells. Four biological replicates were used for **(+)-JQ1**. Expression was normalized to GAPDH for each replicate. Data were visualized with the expression value for each gene in the DMSO normalized to 1, and other genes and treatments were depicted as fold-change relative to DMSO.

BRD4-NUT RNA Interference. These studies were performed as described[64].

Xenograft Efficacy Studies. NMC 797 xenografts were established by injecting NMC 797 cells (10^7) in 30 % Matrigel (BD Biosciences) into the flank of 6 week-old female NCr nude mice (Charles River Laboratories). Twelve days after injection, mice with measureable tumors were divided into cohorts to be treated with **JQ1** at 50 mg kg^{-1} IP or vehicle (5 % DMSO in 5 % dextrose). For FDG-PET studies, mice with established tumors measuring approximately 1 cm in the largest linear dimension underwent baseline CT/PET imaging 1 h after injection of 250 μCi of FDG (Pre-treatment). Mice were then treated with four daily doses of 50 mg kg^{-1} of racemic **JQ1** by intraperitoneal injection. Two hours after the fourth dose of **JQ1** or vehicle, mice underwent repeat FDG-PET

imaging (Post-treatment). The integrated signal encompassed within the entire tumor volume is expressed as the percent of injected dose per gram (% ID/gm). Tumors were fixed in 10 % buffered formalin for histopathological analysis. For tumor caliper studies, the average size of tumors in the **JQ1** treatment group (n = 8) and vehicle group (n = 7) were similar (63.8 ± 17.1 and 73.6 ± 14.4 mm^3 respectively) at the start of treatment. Animals were followed daily for clinical symptoms. Tumor measurements were assessed by caliper measurements, and volume calculated using the formula Vol = 0.5 x L x W^2. After 2 weeks of treatment, all mice were humanely euthanized, and tumors were fixed in 10 % formalin for histopathological examination. Statistical significance of tumor volumes was calculated by two-sided Students t-test.

Primary NMC Xenograft Studies. A primary xenograft model of NMC was established by injecting NCr nude mice with primary cells (10^7 cells in 100 µl of 30 % Matrigel in 70 % PBS) collected from malignant pleural fluid obtained with IRB approval and informed consent from a patient at the Dana-Farber Cancer Institute and Brigham & Women's Hospital. As above, four mice with established tumors measuring approximately 1 cm in the largest linear dimension underwent baseline CT/PET imaging 1 h after injection of 250 µCi of FDG (Pre-treatment). Mice were then treated with four daily doses of 50 mg kg^{-1} of **(+)-JQ1** by intraperitoneal injection. Animals were followed daily for clinical symptoms. Two hours after the fourth dose of **(+)-JQ1** or vehicle, mice underwent repeat FDG-PET imaging (Post-treatment). The integrated signal encompassed within the entire tumor volume is expressed as the percent of injected dose per gram (%ID/gm). Tumors were fixed in 10 % buffered formalin for histopathological analysis. At the conclusion of the study, all mice were humanely euthanized, and tumors were fixed in 10 % formalin for histopathological examination.

Survival (30 days) studies performed with NMC Per403 and 11060 xenografts were initiated as above. For these studies, **(+)-JQ1** was administered at a dose of 50 mg kg^{-1} by

daily intraperitoneal injection. The average size of tumors in the **(+)-JQ1** treatment group (n = 10) and vehicle group (n = 10) were similar at the start of treatment. Animals were followed daily for clinical symptoms. Tumor measurements were assessed by caliper measurements, and volume calculated using the formula Vol = $0.5xLxW^2$. Statistical significance of tumor volumes was calculated by two-sided Students t-test. Comparative survival analysis was performed using the Log-rank (Mantel-Cox) Test, and data were presented as a Kaplain-Meier plot annotated with a measure of statistical significance (p-value).All animal studies were approved by the IACUC of the DFCI.

Instrumentation. Proton and carbon-13 nuclear magnetic resonance (^{1}H NMR and ^{13}C NMR) spectra were recorded with a Varian inverse probe 600 INOVA spectrometer at the Harvard Medical School East Quad NMR Facility. Chemical shifts are recorded in parts per million on the δ scale and are referenced from the residual protium in the NMR solvent ($CHCl_3$: δ 7.24) for ^{1}H NMR, the carbon resonances of the solvent ($CDCl_3$: δ 77.2) for ^{13}C NMR respectively. Data is reported as follows: chemical shift [multiplicity (s = singlet, d = doublet, t = triplet, q = quartet, m = multiplet, br = broad), coupling constant(s) in Hertz, integration]. High resolution mass spectra (HRMS) were recorded on a Bruker APEX 4.7 Tesla FTMS spectrometer using electrospray ion source (ESI) at the Instrumentation Facility of the Department of Chemistry, Massachusetts Institute of Technology. The intermediates and final product were purified with a CombiFlash RF system (Teledyne Isco). Organic solutions were concentrated on Büchi R-205 rotary evaporators. The enantiomeric purities were checked with Berger Supercritical Fluid Chromatography (SFC) and an AS-H column. The enantiomeric preparative purification was performed with Agilent High Pressure Liquid Chromatography and an OD-H column (Broad Institute of Harvard and MIT).

Receptor Profiling Studies. Selectivity profiling (ExpresSProfile) was performed on **JQ1** against 55 ligand receptors, ion channels and transport proteins by CEREP using

Manufacturer's protocols. Data were analyzed in Microsoft Excel (Microsoft Corp.) and GraphPad Prism 5.02.

Pharmacokinetic Studies in Mice. Male CD1 mice (24 – 29 gm; SLAC Laboratory Animal Co.) were treated with a single dose of **(+)-JQ1** at 5 mg kg^{-1} for intravenous tail vein injection studies and 10 mg kg^{-1} for oral gavage studies. Approximately 150 µl of blood were taken from animals by retro-orbital puncture under anesthesia with Isoflurane into EDTA tubes at pre-specified time intervals: 0.033, 0.083, 0.25, 0.5, 1, 2, 4, 5, 8 and 24 hours. Three animals were analyzed per time point. Blood samples were put on ice and centrifuged to obtain plasma samples (2000 x.g, 5 min under 4 °C) within 15 minutes post-sampling. Plasma samples were stored at approximately -70 °C until analysis was performed. Mice were provided free access to food and water throughout the study. Compound was formulated for intravenous injection in 10 % DMSO and 10 % HP-β-CD. Pharmcokinetic studies and pharmacologic assay development was performed at ChemPartner (Shanghai, CHINA). Data were analyzed by J.E.B. using Microsoft Excel and GraphPad Prism 5.02.

SYNTHETIC PROCEDURES

Scheme S1. Synthesis of the racemic bromodomain inhibitor **(±)-JQ1**.

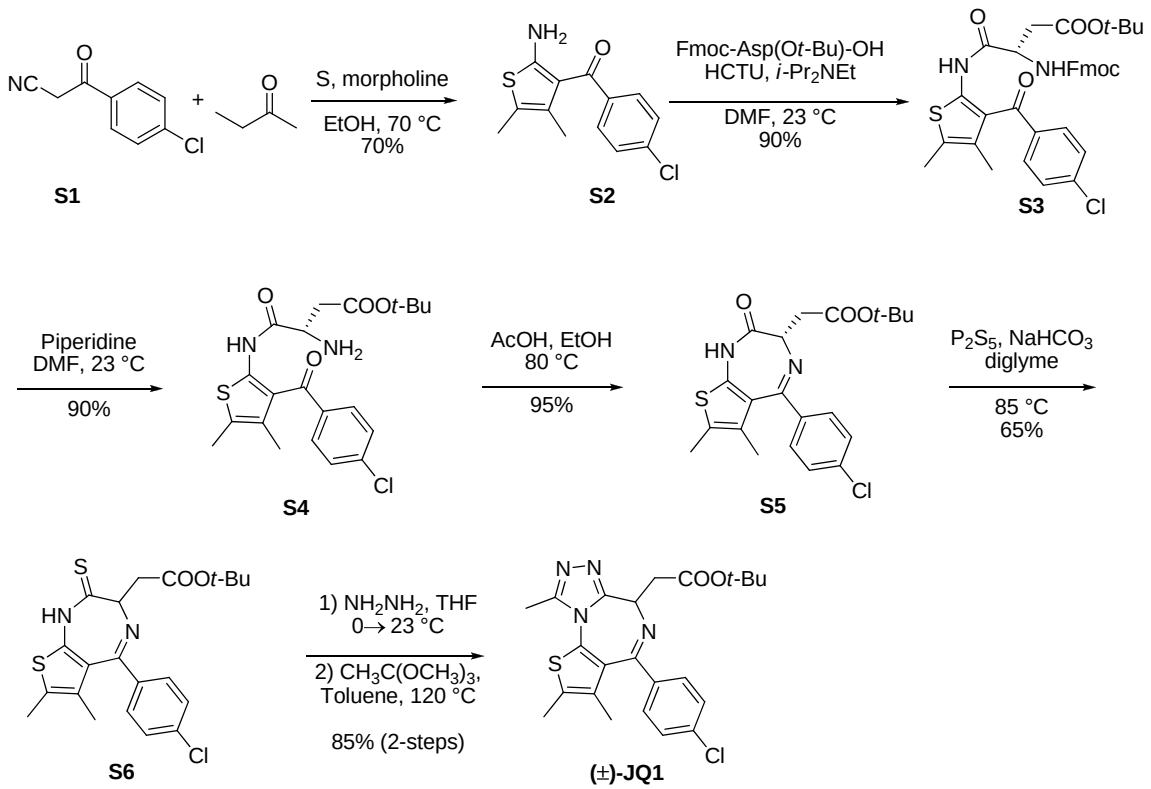

(2-amino-4,5-dimethylthiophen-3-yl)(4-chloropheyl)methanone (**S2**)

Sulfur (220 mg, 6.9 mmol, 1.00 equiv) was added as a solid to a solution of 4-chlorobenzoyl acetonitrile S1 (1.24 g, 6.9 mmol, 1 equiv), 2-butanone (0.62 ml, 6.9 mmol, 1.00 equiv), and morpholine (0.60 ml, 6.9 mmol, 1.00 equiv) in ethanol (20 ml, 0.35 M) at 23 ºC[65]. The mixture was then heated to 70 ºC. After 12 h, the reaction mixture was cooled to 23 ºC and poured into brine (100 ml). The aqueous layer was extracted with ethyl acetate (3 x 50 ml). The combined organic layers were washed with brine (50 ml), were dried over anhydrous sodium sulphate, were filtered, and were concentrated under reduced pressure. The residue was purified by flash column

chromatography (Combiflash RF system, 40 gram silica gel, gradient 0 to 100 % ethyl acetate-hexanes) to afford **S2** (1.28 g, 70 %) as yellow solid.

^{1}H NMR (600 MHz, $CDCl_3$, 25 °C) δ 7.47 (d, *J* = 8.4 Hz, 2H), 7.36 (d, *J* = 8.4 Hz, 2H), 6.40 (s, br, 2H), 2.14 (s, 3H), 1.58 (s, 3H).

^{13}C NMR (150 MHz, $CDCl_3$, 25 °C) δ 191.8, 163.2, 140.3, 136.3, 129.7, 128.7, 128.6, 117.4, 115.6, 15.7, 12.8.

MS(ESI) calc'd for $C_{13}H_{12}ClNOS$ $[M+H]^+$: 266.03, found 266.02 m/z.

TLC (2% MeOH-DCM), *Rf*: 0.72 (UV)

(*S*)-*tert*-Butyl-3-({[(9H-fluoren-9-yl)methoxy]carbonyl}amino)-4-{[3-(4-chlorobenzoyl)-4,5-dimethylthiophen-2-yl]amino}-4-oxobutanoate (**S3**)

(2-(6-Chloro-1H-benzotriazole-1-yo)-1,1,3,3-tetramethylaminium hexafluorophosphate (HCTU) (827 mg, 2.0 mmol, 2.00 equiv), *N*,*N*-diisopropylethylamine (0.72 ml, 4.0 mmol, 4.00 equiv) were added sequentially to a solution of 9-fluorenylmethoxycarbonyl-aspartic acid β-*tert*-butyl ester [Fmoc-Asp(O*t*-Bu)-OH] (864 mg, 2.1 mmol, 2.10 equiv) in *N*,*N*-dimethylformamide (1.5 ml, 1.0 M). The mixture was then stirred at 23 °C for 5 min. **S2** (266 mg, 1.0 mmol, 1 equiv) was then added as a solid. The reaction mixture was stirred at 23 °C. After 16 h, ethyl acetate (20 ml) and brine (20 ml) were added. The two layers were separated, and the aqueous layer was extracted with ethyl acetate (2 x 20 ml). The combined organic layers were washed with brine (30 ml), were dried over with anhydrous sodium sulphate, were filtered, and were concentrated under reduced pressure. The residue was purified by flash column chromatography (Combiflash RF, 40 gram silica gel, gradient 0 to 100 % ethyl acetate-hexanes) to afford **S3** (625 mg, 90 %) as brown oil.

(*S*)-*tert*-butyl 3-amino-4-((3-(4-chlorobenzoyl)-4,5-dimethylthiophen-2-yl)amino)-4-oxobutanoate (**S4**)

Compound **S3** (560 mg, 0.85 mmol, 1 equiv) was dissolved into 20 % piperidine in DMF solution (4.0 ml, 0.22 M) at 23 °C. After 30 min, ethyl acetate (20 ml) and brine (20 ml) were added to the reaction mixture. The two layers were separated, and the aqueous layer was extracted with ethyl acetate (2 x 20 ml). The combined organic layers were washed with brine (3 x 25 ml), were dried over anhydrous sodium sulphate, were filtered, and were concentrated under reduced pressure. The residue was purified by flash column chromatography (Combiflash RF system, 24 gram silica gel, gradient 0 to 100 % ethyl acetate-hexanes) to afford free amine **S4** (370 mg, 90 %) as yellow solid. The enantiomeric purity dropped to 75 % (determined with Berger Supercritical Fluid Chromatography (SFC) using AS-H column).

(*S*)-*tert*-Butyl 2-(5-(4-chlorophenyl)-6,7-dimethyl-2-oxo-2,3-dihydro-1H-thieno[2,3-e][1,4]diazepin-3-yl)acetate (**S5**)

Amino ketone **(S4)** (280 mg, 0.63 mmol) was dissolved in 10 % acetic acid ethanol solution (21 ml, 0.03 M). The reaction mixture was heated to 85 °C. After 30 min, all solvents were removed under reduce pressure. The residue was purified by flash column chromatography (Combiflash RF system, 12 gram silica gel, gradient 0 to 100 % ethyl acetate-hexanes) to afford compound **S5** (241 mg, 95 %) as white solid. Enantiomeric purity of **S5** was 67 % (determined with Berger Supercritical Fluid Chromatography (SFC) using an AS-H column).

tert-Butyl 2-(5-(4-chlorophenyl)-6,7-dimethyl-2-thioxo-2,3-dihydro-1H-thieno[2,3-e][1,4]diazepin-3-yl)acetate (**S6**)

Phosphorus pentasulfide (222 mg, 1.0 mmol, 2.00 equiv), sodium bicarbonate (168 mg, 2.0 mmol, 4.00 equiv) were added sequentially to a solution of S5 (210 mg, 0.5 mmol, 1 equiv) in diglyme (1.25 ml, 0.4M). The reaction mixture was heated to 90 °C. After 16 h, brine (20 ml) and ethyl acetate (35 ml) were added. The two layers were separated, and the aqueous layer was extracted with ethyl acetate (3 x 30 ml). The combined organic layers were washed with brine (2 x 15 ml), were dried over anhydrous sodium sulphate, were filtered, and were concentrated under reduced pressure. The residue was purified by flash column chromatography (Combiflash RF system, 24 gram silica gel, gradient 0 to 100 % ethyl acetate-hexanes) to afford **S6** (141 mg, 65 %) as brown solid with recover **S5** (73 mg, 34 %).

tert-Butyl 2-(4-(4-chlorophenyl)-2,3,9-trimethyl-6H-thieno[3,2-f][1,2,4]triazolo[4,3-a][1,4]diazepin-6-yl)acetate [(±)-**JQ1**]

Hydrazine (0.015 ml 0.45 mmol, 1.25 equiv) was added to a solution of S6 (158 mg, 0.36 mmol, 1 equiv) in THF (2.6 ml, 0.14 M) at 0 °C. The reaction mixture was warmed to 23 °C, and stirred at 23 °C for 1 h. All solvents were removed under reduce pressure. The resulting hydrazine was used directly without purification. The hydrazine was then dissolved in a 2:3 mixture of trimethyl orthoacetate and toluene (6 ml, 0.06 M). The reaction mixture was heated to 120 °C. After 2 h, all the solvents were removed under reduce pressure. The residue was purified by flash column chromatography (Combiflash system, 4 g silica gel, gradient 0 to 100 % ethyl acetate-hexanes) to afford **JQ1** (140 mg, 85 % in 2-steps) as white solid. The reaction condition further epimerized the stereogenic center, resulting in the racemate, **JQ1** (determined with Berger Supercritical Fluid Chromatography (SFC) with an AS-H column).

Scheme S2. Synthesis of enantiomerically enriched (+)-**JQ1**.

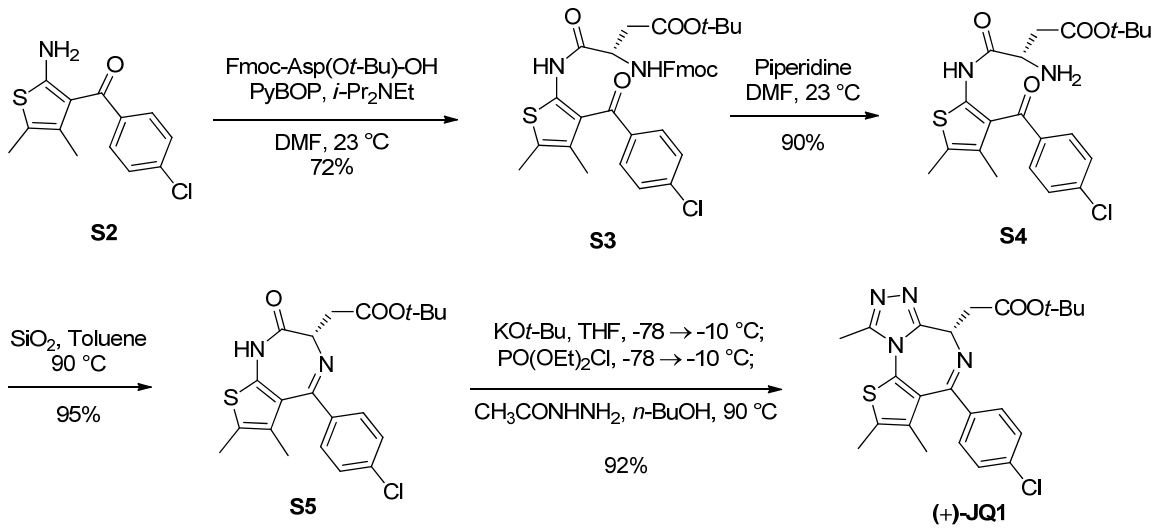

(*S*)-*tert*-Butyl-3-({[(9H-fluoren-9-yl)methoxy]carbonyl}amino)-4-{[3-(4-chlorobenzoyl)-4,5-dimethylthiophen-2-yl]amino}-4-oxobutanoate (**S3**)

(Benzotriazol-1-yloxyl)tripyrrolidinophosphonium (PyBOP) (494 mg, 0.95 mmol, 0.95 equiv), *N*,*N*-diisopropylethylamine (0.50 mL, 2.8 mmol, 2.75 equiv) were added sequentially to a solution of 9-fluorenylmethoxycarbonyl-aspartic acid β-tert-butyl ester [Fmoc-Asp(Ot-Bu)-OH] (411 mg, 1.00 mmol, 1.0 equiv) in *N*,*N*-dimethylformamide (1.0 ml, 1.0 M). The mixture was then stirred at 23 °C for 5 min. **S2** (266 mg, 1.0 mmol, 1 equiv) was then added as solid. The reaction mixture was stirred at 23 °C. After 4 h, ethyl acetate (20 ml) and brine (20 ml) were added. The two layers were separated, and the aqueous layer was extracted with ethyl acetate (2 x 20 ml). The combined organic layers were washed with brine, were dried over with anhydrous sodium sulphate, were filtered, and were concentrated under reduced pressure. The residue was purified by flash column chromatography (Combiflash RF system, 40 gram silica gel, gradient 0 to 100 % ethyl acetate-hexanes) to afford **S3** (452 mg, 72 %) as brown oil.

^{1}H NMR (600 MHz, $CDCl_3$, 25 °C) δ 11.7 (s, br, 1H), 7.75 (d, *J* = 7.8 Hz, 2H), 7.63 (dd, *J* = 7.2, 18 Hz, 2 H), 7.43 (d, *J* = 8.4 Hz, 2H), 7.37 (t, *J* = 7.2 Hz, 2H), 7.32 (d, *J* = 8.4 Hz, 2H), 7.26-7.19 (m, 2H), 6.10 (d, *J* = 9.0 Hz, 1H), 4.78 (s, br, 1H), 4.64 (s, br,

1H), 4.23-4.32 (m, 2H), 3.14 (d, *J* = 18 Hz, 1H), 2.73 (d, *J* = 18 Hz, 1H), 2.25 (s, 3H), 1.67 (s, 3H), 1.43 (s, 9H).

TLC (10% EtOAc-Hexane), *Rf*: 0.24 (UV)

MS(ESI) calc'd for $C_{36}H_{36}ClN_2O_6S$ $[M+H]^+$: 659.19, found 659.20 m/z.

$[\alpha]^{22}_D$ = + 17.2 (*c* 0.5, $CHCl_3$)

(*S*)-*tert*-butyl 3-amino-4-((3-(4-chlorobenzoyl)-4,5-dimethylthiophen-2-yl)amino)-4-oxobutanoate (**S4**)

Compound **S3** (310 mg, 0.47 mmol, 1 equiv) was dissolved into 20 % piperidine in DMF solution (2.2 ml, 0.22 M) at 23 °C. After 30 min, ethyl acetate (20 ml) and brine (20 ml) were added to the reaction mixture. The two layers were separated, and the aqueous layer was extracted with ethyl acetate (2 x 20 ml). The combined organic layers were washed with brine (3 x 25 ml), were dried over anhydrous sodium sulphate, were filtered, and were concentrated under reduced pressure. The residue was purified by flash column chromatography (Combiflash RF system, 24 gram silica gel, gradient 0 to 100 % ethyl acetate-hexane) to afford free amine **S4** (184 mg, 90 %) as yellow solid. The enantiomeric purity was 91 % (checked with Berger Supercritical Fluid Chromatography (SFC) using an AS-H column).

^{1}H NMR (600 MHz, $CDCl_3$, 25 °C) δ 12.1 (s, br, 2H), 7.57 (d, *J* = 8.4 Hz, 2H), 7.41 (d, *J* = 8.4 Hz, 2H), 3.86 (s, br, 1H), 2.93-2.84 (m, 1H), 2.78-2.66 (m, 1H), 2.26 (s, 3H), 1.71 (s, 3H), 1.42 (s, 9H).

TLC (25% EtOAc-Hexane), *Rf*: 0.40 (UV)

MS(ESI) calc'd for $C_{21}H_{25}ClN_2O_4S$ $[M+H]^+$: 437.12, found 437.13 m/z.

$[\alpha]^{22}_D$ = + 25.2 (*c* 0.5, $CHCl_3$)

(*S*)-*tert*-Butyl 2-(5-(4-chlorophenyl)-6,7-dimethyl-2-oxo-2,3-dihydro-1H-thieno[2,3-e][1,4]diazepin-3-yl)acetate (**S5**)Amino ketone **(S4**) (184 mg, 0.42 mmol) was dissolved in toluene (10 ml, 0.04 M). Silica gel (300 mg) was added, and the reaction mixture was heated to 90 °C. After 3 h, the reaction mixture was cooled to 23 °C. The silica gel was filtered, and washed with ethyl acetate. The combined filtrates were concentrated. The residue was purified by flash column chromatography (Combiflash RF system, 12 gram silica gel, gradient 0 to 100 % ethyl acetate-hexanes) to afford compound **S5** (168 mg, 95 %) as white solid. Enantiomeric purity of **S5** was 90 % (determined with Berger Supercritical Fluid Chromatography (SFC) using an AS-H column).

^{1}H NMR (600 MHz, $CDCl_3$, 25 °C) δ 9.03 (s, br, 1H), 7.35 (d, *J* = 8.4 Hz, 2H), 7.25 (d, *J* = 8.4 Hz, 2H), 4.13 (t, *J* = 7.2 MHz, 1H), 3.31-3.22 (m, 1H), 3.04-2.99 (m, 1H), 2.21 (s, 3H), 1.52 (s, 3H), 1.41 (s, 9H).

^{13}C NMR (150 MHz, $CDCl_3$, 25 °C) δ 171.3, 169.5, 141.2, 137.1, 136.6, 130.4, 129.9, 129.3, 128.8, 128.5, 127.9, 126.8, 80.9, 61.5, 37.7, 28.4, 14.7, 13.1.

MS(ESI) calc'd for $C_{21}H_{24}ClN_2O_3S$ $[M+H]^+$: 418.11, found 418.10 m/z.

TLC (25% EtOAc-Hexanes), *Rf*: 0.50 (UV)

$[\alpha]^{22}_D$ = + 37 (*c* 0.5, $CHCl_3$)

(*S*)-*tert*-Butyl 2-(4-(4-chlorophenyl)-2,3,9-trimethyl-6H-thieno[3,2-f][1,2,4]triazolo[4,3-a][1,4]diazepin-6-yl)acetate [(+)-**JQ1**]

Potassium *tert*-butoxide (1.0 M solution in THF, 0.3 mL, 0.30 mmol, 1.10 equiv) was added to a solution **S5** (114 mg, 0.27 mmol, 1 equiv) in THF (1.8 ml, 0.15 M) at -78 °C. The reaction mixture was warmed to -10 °C, and stirred at 23 °C for 30 min. The reaction mixture was cooled to -78 °C. Diethyl chlorophosphate (0.047 mL, 0.32 mmol, 1.20 equiv) was added to reaction mixture[66]. The resulting mixture was warmed to -10 °C over 45 min. Acetic hydrazide (30 mg, 0.40 mmol, 1.50 equiv) was added to reaction mixture. The reaction mixture was stirred at 23 °C. After 1 h, 1-butanol (2.25 ml) was added to reaction mixture, which was heated to 90 °C. After 1 h, all solvents were removed under reduce pressure. The residue was purified with flash column chromatography (Combiflash system, 4 g silica gel, gradient 0 to 100 % ethyl acetate-hexanes) to afford (+)-**JQ1** (114 mg, 92 %) as white solid with 90 % enantiomeric purity (determined with Berger Supercritical Fluid Chromatography (SFC) using AS-H column, 85 % hexanes- methanol, 210 nm, t_R (R-enantiomer) = 1.59 min, t_R (S-enantiomer) = 3.67 min). The product was further purified by chiral preparative HPLC (Agilent High Pressure Liquid Chromatography using an OD-H column) to provide the *S*-enantiomer in greater than 99 % ee.

^{1}H NMR (600 MHz, $CDCl_3$, 25 °C) δ 7.39 (d, *J* = 8.4 Hz, 2H), 7.31 (d, *J* = 8.4 Hz, 2H), 4.54 (t, *J* = 6.6 MHz, 1H), 3.54-3.52 (m, 2H), 2.66 (s, 3H), 2.39 (s, 3H), 1.67 (s, 3H), 1.48 (s, 9H).

^{13}C NMR (150 MHz, $CDCl_3$, 25 °C) δ 171.0, 163.8, 155.7, 150.0, 136.9, 131.1, 130.9, 130.6, 130.3, 128.9, 81.2, 54.1, 38.1, 28.4, 14.6, 13.5, 12.1.

HRMS(ESI) calc'd for $C_{21}H_{26}ClN_2O_3S$ $[M+H]^+$: 457.1460, found 457.1451 m/z.

TLC (EtOAc), *Rf*: 0.32 (UV)

$[\alpha]^{22}_{D}$ = + 55 (*c* 0.5, $CHCl_3$)

(–)-**JQ1** was synthesized in a similar manner, employing Fmoc-D-Asp(O*t*-Bu)-OH as a starting material, and was further purified by chiral preparative HPLC (Agilent High Pressure Liquid Chromatography using an OD-H column) to afford the *R*-enantiomer in greater than 99 % ee. $[\alpha]^{22}_{D}$ = – 52 (*c* 0.5, $CHCl_3$)

Enantiomeric purity determination of (*S*)-JQ1 and (*R*)-JQ1 via chiral HPLC

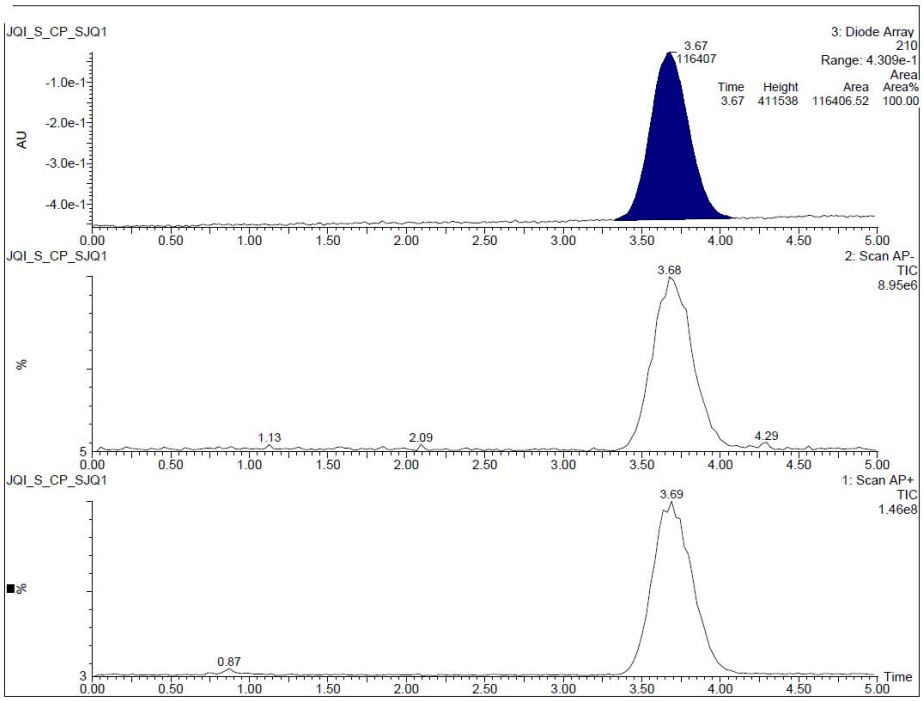

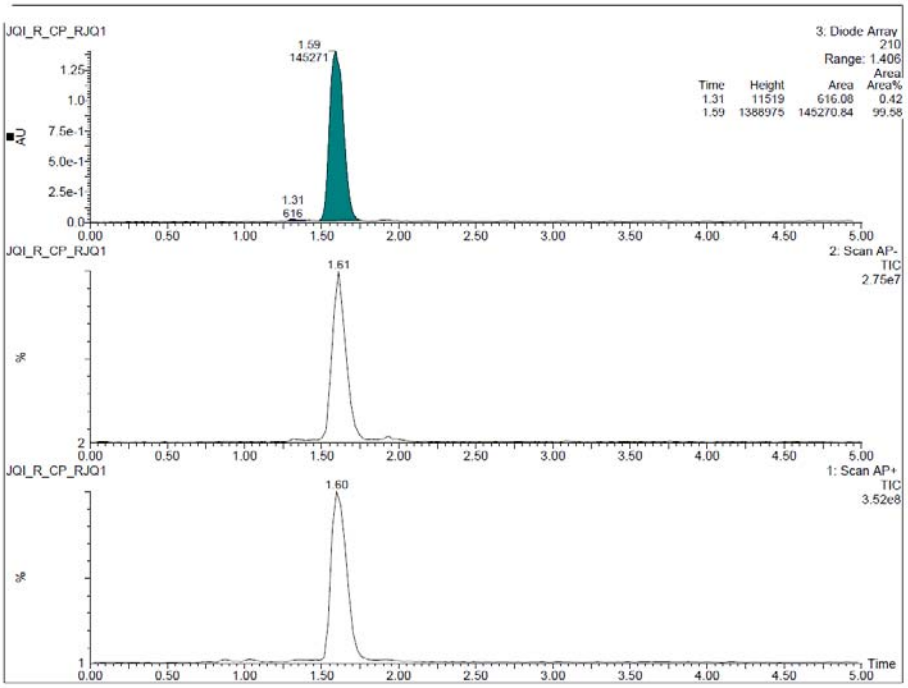

^{1}H NMR and ^{13}C NMR of JQ1

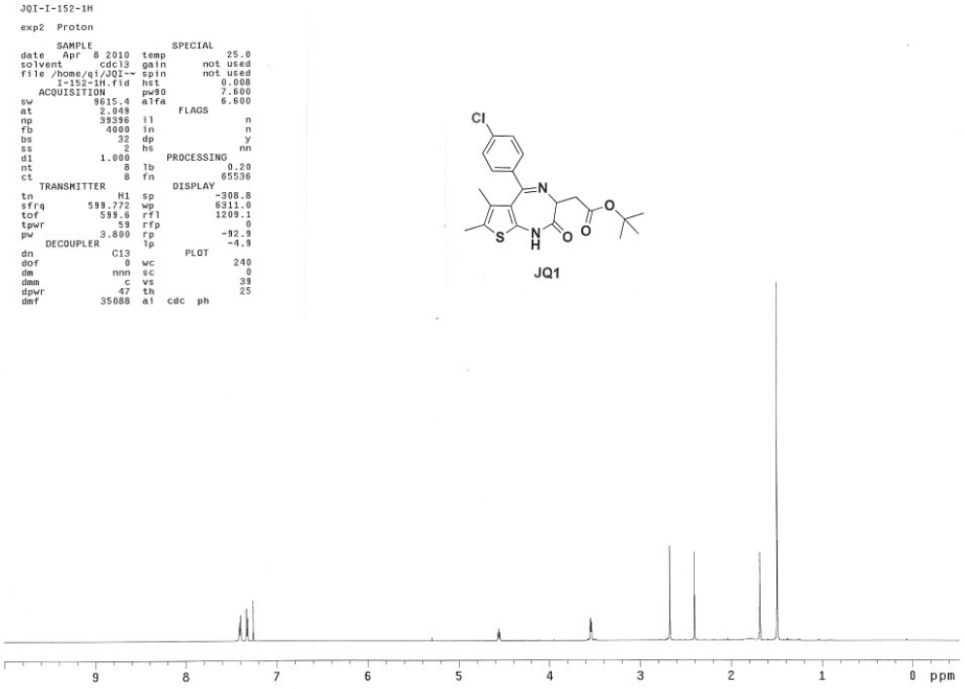

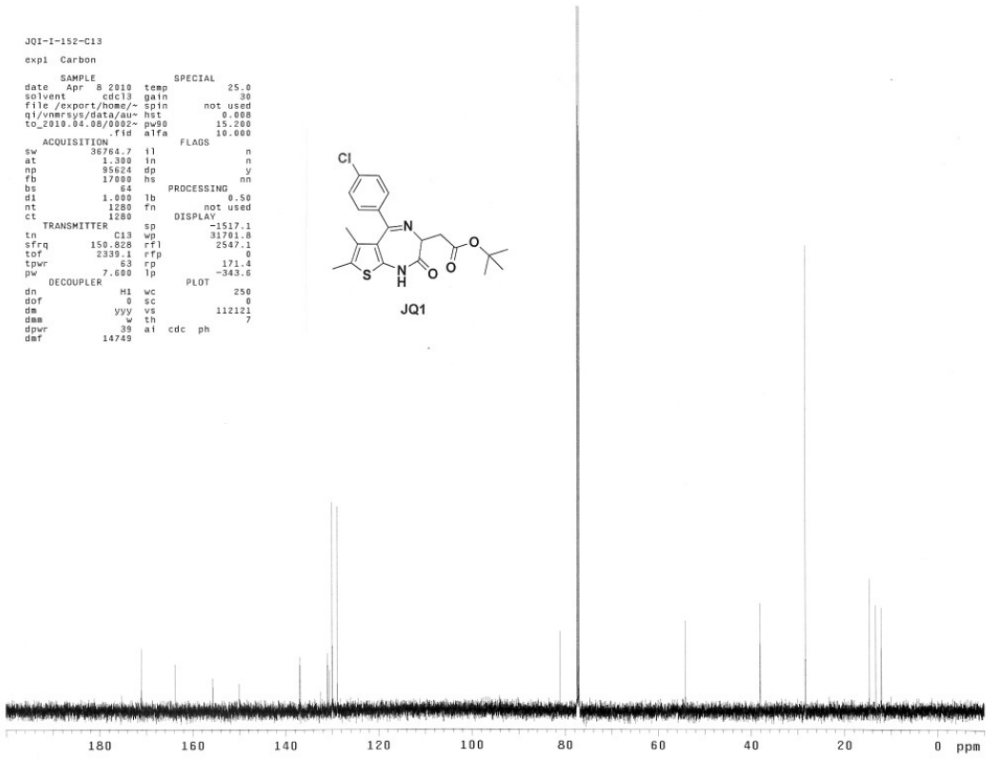

Supplementary Table 1 | Bromodomain constructs expressed and purified for Selectivity Screening Panel. All constructs were subcloned into a bacterial vector (pNIC28-Bsa4, GenBank: EF198106.1) and were purified on Ni-NTA. The final buffer was exchanged to 25 mM HEPES pH 7.5, 150 mM NaCl and 5% glycerol on NAP10 columns (Amersham Biosciences).

Name	Genbank ID	Expressed sequence	Expression Cell Line
ASH1L	gi|8922081	MHHHHHHSSGVDLGTENLYFQSMAEENIEVARAARLAQIFKE ICDGIISYKDSSRQALAAPLLNLPPKKKNADYYEKISDPLDL ITIEKQILTGYYKTVEAFDADMLKVFRNAEKYYGRKSPVGRD VCRLRKAYYNARHEASAQIDEIVGETASE	BL21(DE3)-R3-pRARE2
ATAD2	gi|24497618	MHHHHHHSSGVDLGTENLYFQSMQEEDTFRELRIFLRNVTHR LAIDKRFRVFTKPVDPDEVPDYVTVIKQPMDLSSVISKIDLH KYLTVKDYLRDIDLICSNALEYNPDRDPGDRLIRHRACALRD TAYAIIKEELDEDFEQLCEEIQESR	BL21(DE3)-R3
BAZ2B	gi|7304923	MHHHHHHSSGVDLGTENLYFQSMSVKKPKRDDSKDLALCSMI LTEMETHEDAWPFLLPVNLKLVPGYKKVIKKPMDFSTIREKL SSGQYPNLETFALDVRLVFDNCETFNEDDSDIGRAGHNMRKY FEKKWTDTFKVS	BL21(DE3)-R3-pRARE2
BRD1	gi|11321642	MHHHHHHSSGVDLGTENLYFQSMEQVAMELRLTPLTVLLRSV LDQLQDKDPARIFAQPVSLKEVPDYLDHIKHPMDFATMRKRL EAQGYKNLHEFEEDFDLIIDNCMKYNARDTVFYRAAVRLRDQ GGVVLRQARREVDSIGLEEASGMHLPERPA	BL21(DE3)-R3-pRARE2
BRD2(1)	gi|4826806	MHHHHHHSSGVDLGTENLYFQSMKPGRVTNQLQYLHKVVMKA LWKHQFAWPFRQPVDAVKLGLPDYHKIIKQPMDMGTIKRRLE NNYYWAASECMQDFNTMFTNCYIYNKPTDDIVLMAQTLEKIF LQKVASMPQEEQELVVTIPKN	BL21(DE3)-R3
BRD2(2)	gi|4826806	MHHHHHHSSGVDLGTENLYFQSMEQLKHCNGILKELLSKKHA AYAWPFYKPVDASALGLHDYHDIIKHPMDLSTVKRKMENRDY RDAQEFAADVRLMFSNCYKYNPPDHDVVAMARKLQDVFEFRY	BL21(DE3)-R3-pRARE2

		AKMPD	
BRD3(1)	gi|11067749	MHHHHHHSSGVDLGTENLYFQSMPEVSNPSKPGRKTNQLQYMQNVVVKTLWKHQFAWPFYQPVDAIKLNLPDYHKIIKNPMDMGTIKKRLENNYYWSASECMQDFNTMFTNCYIYNKPTDDIVLMAQALEKIFLQKVAQMPQEE	BL21(DE3)-R3-pRARE2
BRD3(2)	gi|11067749	MHHHHHHSSGVDLGTENLYFQSMGKLSEHLRYCDSILREMLSKKHAAYAWPFYKPVDAEALELHDYHDIIKHPMDLSTVKRKMDGREYPDAQGFAADVRLMFSNCYKYNPPDHEVVAMARKLQDVFEMRFAKMP	BL21(DE3)-R3-pRARE2
BRD4(1)	gi|19718731	MHHHHHHSSGVDLGTENLYFQSMNPPPPETSNPNKPKRQTNQLQYLLRVVLKTLWKHQFAWPFQQPVDAVKLNLPDYYKIIKTPMDMGTIKKRLENNYYWNAQECIQDFNTMFTNCYIYNKPGDDIVLMAEALEKLFLQKINELPTEE	BL21(DE3)-R3-pRARE2
BRD4(2)	gi|19718731	MHHHHHHSSGVDLGTENLYFQSMKDVPDSQQHPAPEKSSKVSEQLKCCSGILKEMFAKKHAAYAWPFYKPVDVEALGLHDYCDIIKHPMDMSTIKSKLEAREYRDAQEFGADVRLMFSNCYKYNPPDHEVVAMARKLQDVFEMRFAKMPDE	BL21(DE3)-R3-pRARE2
BRD9	gi|57770383	MHHHHHHSSGVDLGTENLYFQSMLKLSAENESTPIQQLLEHFLRQLQRKDPHGFFAFPVTDAIAPGYSMIIKHPMDFGTMKDKIVANEYKSVTEFKADFKLMCDNAMTYNRPDTVYYKLAKKILHAGFKMMSKERLLALKRSMSFMQDMDFSQ	BL21(DE3)-R3
BRDT(1)	gi|46399198	MHHHHHHSSGVDLGTENLYFQSMNTKKNGRLTNQLQYLQKVVLKDLWKHSFSWPFQRPVDAVKLQLPDYYTIIKNPMDLNTIKKRLENKYYAKASECIEDFNTMFSNCYLYNKPGDDIVLMAQALEKLFMQKLSQMPQEE	BL21(DE3)-R3-pRARE2
BRPF1	gi|51173720	MHHHHHHSSGVDLGTENLYFQSMEMQLTPFLILLRKTLEQLQEKDTGNIFSEPVPLSEVTELDEVPDYLDHIKKPMDFFTMKQNLEAYRYLNFDDFEEDFNLIVSNCLKYNAKDTIFYRAAVRLREQGGAVLRQARRQAEKMG	BL21(DE3)-R3
CECR2	gi|148612882	MHHHHHHSSGVDLGTENLYFQSMPNSPMREEKKTKDLFELDDDFTAMYKVLDVVKAHKDSWPFLEPVDESYAPNYYQIIKAPMD	BL21(DE3)-R3

		ISSMEKKLNGGLYCTKEEFVNDMKTMFRNCRKYNGESSEYTK MSDNLERCFHRAMMKHFPGED	
CREBBP	gi|4758056	MHHHHHHSSGVDLGTENLYFQSMRKKIFKPEELRQALMPTLE ALYRQDPESLPFRQPVDPQLLGIPDYFDIVKNPMDLSTIKRK LDTGQYQEPWQYVDDVWLMFNNAWLYNRKTSRVYKFCSKLAE VFEQEIDPVMQSLG	BL21(DE3)-R3
EP300	gi|50345997	MHHHHHHSSGVDLGTENLYFQSMAPGQSKKKIFKPEELRQAL MPTLEALYRQDPESLPFRQPVDPQLLGIPDYFDIVKSPMDLS TIKRKLDTGQYQEPWQYVDDIWLMFNNAWLYNRKTSRVYKYC SKLSEVFEQEIDPVMQSLG	BL21(DE3)-R3
FALZ	gi|38788274	MHHHHHHSSGVDLGTENLYFQSMSTEDAMTVLTPLTEKDYEG LKRVLRSLQAHKMAWPFLEPVDPNDAPDYYGVIKEPMDLATM EERVQRRYYEKLTEFVADMTKIFDNCRYYNPSDSPFYQCAEV LESFFVQKLKGFKASRSH	BL21(DE3)-R3
GCN5L2	gi|10835101	MHHHHHHSSGVDLGTENLYFQSMELKDPDQLYTTLKNLLAQI KSHPSAWPFMEPVKKSEAPDYYEVIRFPIDLKTMTERLRSRY YVTRKLFVADLQRVIANCREYNPPDSEYCRCASALEKFFYFK LKEGGLIDK	BL21(DE3)-R3
KIAA1240	gi|51460532	MHHHHHHSSGVDLGTENLYFQSMEDQEENTLRELRLFLRDVT KRLATDKRFNIFSKPVDIEEVSDYLEVIKEPMDLSTVITKID KHNYLTAKDFLKDIDLICSNALEYNPDKDPGDKIIRHRACTL KDTAHAIIAAELDPEFNKLCEEIKEARIKRG	BL21(DE3)-R3
LOC93349	gi|134133279	MHHHHHHSSGVDLGTENLYFQSMRNLDECEVCRDGGELFCCD TCSRVFHEDCHIPPVESEKTPWNCIFCRMKESPGSQQCCQES EVLERQMCPEEQLKCEFLLLKVYCCSESSFFAKIPYYYYIRE ACQGLKEPMWLDKIKKRLNEHGYPQVEGFVQDMRLIFQNHRA SYKYKDFGQMGLRLEAEFEKDFKEVFAIQETNGNS	BL21(DE3)-R3
PB1(1)	gi|30794372	MHHHHHHSSGVDLGTENLYFQSMHHSVSTPGPSRKRRRLSNL PTVDPIAVCHELYNTIRDYKDEQGRLLCELFIRAPKRRNQPD YYEVVSQPIDLMKIQQKLKMEEYDDVNLLTADFQLLFNNAKS YYKPDSPEYKAACKLWDLYLRTRNEFVQKGE	BL21(DE3)-R3-pRARE2

PB1(2)	gi|30794372	MHHHHHHSSGVDLGTENLYFQSMSPAYLKEILEQLLEAIVVATNPSGRLISELFQKLPSKVQYPDYYAIIKEPIDLKTIAQRIQNGSYKSIHAMAKDIDLLAKNAKTYNEPGSQVFKDANSIKKIFYMKKAEIEHHE	BL21(DE3)-R3-pRARE2
PB1(3)	gi|30794372	MHHHHHHSSGVDLGTENLYFQSMQLYDTVRSCRNNQGQLIAEPFYHLPSKKKYPDYYQQIKMPISLQQIRTKLKNQEYETLDHLECDLNLMFENAKRYNVPNSAIYKRVLKLQQVMQAKKKELARRDDIE	BL21(DE3)-R3-pRARE2
PB1(5)	gi|30794372	MHHHHHHSSGVDLGTENLYFQSMSGISPKKSKYMTPMQQKLNEVYEAVKNYTDKRGRRLSAIFLRLPSRSELPDYYLTIKKPMDMEKIRSHMMANKYQDIDSMVEDFVMMFNNACTYNEPESLIYKDALVLHKVLLETRRDLEGD	BL21(DE3)-R3-pRARE2
PB1(6)	gi|30794372	MHHHHHHSSGVDLGTENLYFQSMNVTLLIQELIHNLFVSVMSHQDDEGRCYSDSLAEIPAVDPNFPNKPPLTFDIIRKNVENNRYRRLDLFQEHMFEVLERARRMNRTDSEIYEDAVELQQFFIKIRDELCKNGEILLSPALSYTTKHLHNDVEKERKEKLPKEIEED	BL21(DE3)-R3-pRARE2
PCAF	gi|40805843	MHHHHHHSSGVDLGTENLYFQSMGKEKSKEPRDPDQLYSTLKSILQQVKSHQSAWPFMEPVKRTEAPGYYEVIRFPMDLKTMSERLKNRYYVSKKLFMADLQRVFTNCKEYNPPESEYYKCANILEKFFFSKIKEAGLID	BL21(DE3)-R3
PHIP(2)	gi|34996489	MHHHHHHSSGVDLGTENLYFQSMSLIYKPLDGEWGTNPRDEECERIVAGINQLMTLDIASAFVAPVDLQAYPMYCTVVAYPTDLSTIKQRLENRFYRRVSSLMWEVRYIEHNTRTFNEPGSPIVKSAKFVTDLLLHFIKDQTCYNIIPLYNSMKKKVLSDSEDEE	BL21(DE3)-R3-pRARE2
SMARCA2	gi|48255900	MHHHHHHSSGVDLGTENLYFQSMRRGRPPAEKLSPNPPKLTKQMNAIIDTVINYKDRCNVEKVPSNSQLEIEGNSSGRQLSEVFIQLPSRKELPEYYELIRKPVDFKKIKERIRNHKYRSLGDLEKDVMLLCHNAQTFNLEGSQIYEDSIVLQSVFKSARQKIAKEEE	BL21(DE3)-R3-pRARE2
SMARCA4	gi|21071056	MHHHHHHSSGVDLGTENLYFQSMAEKLSPNPPNLTKKMKKIVDAVIKYKDSSSGRQLSEVFIQLPSRKELPEYYELIRKPVDFKKIKERIRNHKYRSLNDLEKDVMLLCQNAQTFNLEGSLIYEDS	BL21(DE3)-R3-pRARE2

		IVLQSVFTSVRQKIEKEDDSEGEESEEEEE	
SP140	gi|52487219	MHHHHHHSSGVDLGTENLYFQSMRNLDECEVCRDGGELFCCD TCSRVFHEDCHIPPVEAERTPWNCIFCRMKESPGSQQCCQES EVLERQMCPEEQLKCEFLLLKVYCCSESSFFAKIPYYYYIRE ACQGLKEPMWLDKIKKRLNEHGYPQVEGFVQDMRLIFQNHRA SYKYKDFGQMGFRLEAEFEKNFKEVFAIQE	BL21(DE3)-R3-pRARE2
TAF1(1)	gi|20357585	MHHHHHHSSGVDLGTENLYFQSMRRTDPMVTLSSILESIIND MRDLPNTYPFHTPVNAKVVKDYYKIITRPMDLQTLRENVRKR LYPSREEFREHLELIVKNSATYNGPKHSLTQISQSMLDLCDE KLKEKEDKLARLEKAINPLLDDDD	BL21(DE3)-R3-pRARE2
TAF1(2)	gi|20357585	MHHHHHHSSGVDLGTENLYFQSMDDDQVAFSFILDNIVTQKM MAVPDSWPFHHPVNKKFVPDYYKVIVNPMDLETIRKNISKHK YQSRESFLDDVNLILANSVKYNGPESQYTKTAQEIVNVCYQT LTEYDEHLTQLEKDICTAKEAALEEAELESLD	BL21(DE3)-R3-pRARE2
TAF1L(1)	gi|24429572	MHHHHHHSSGVDLGTENLYFQSMVTLSSILESIINDMRDLPN THPFHTPVNAKVVKDYYKIITRPMDLQTLRENVRKCLYPSRE EFREHLELIVKNSATYNGPKHSLTQISQSMLDLCDEKLKEKE DKLARLEKAINPLLDDDD	BL21(DE3)-R3-pRARE2
TAF1L(2)	gi|24429572	MHHHHHHSSGVDLGTENLYFQSMQVAFSFILDNIVTQKMMAV PDSWPFHHPVNKKFVPDYYKMIVNPVDLETIRKNISKHKYQS RESFLDDVNLILANSVKYNGPESQYTKTAQEIVNICYQTITE YDEHLTQLEKDICTAKEAALEEAELESLD	BL21(DE3)-R3-pRARE2
TIF1	gi|14971415	MHHHHHHSSGVDLGTENLYFQSMGLVKLTPIDKRKCERLLLF LYCHEMSLAFQDPVPLTVPDYYKIIKNPMDLSTIKKRLQEDY SMYSKPEDFVADFRLIFQNCAEFNEPDSEVANAGIKLENYFE ELLKNLYPEKRFPKPE	BL21(DE3)-R3-pRARE2
TRIM28	gi|5032179	MHHHHHHSSGVDLGTENLYFQSMGTLDDSATICRVCQKPGDL VMCNQCEFCFHLDCHLPALQDVPGEEWSCSLCHVLPDLKEED GSLSLDGADSTGVVAKLSPANQRKCERVLLALFCHEPCRPLH QLATDSTFSLDQPGGTLDLTLIRARLQEKLSPPYSSPQEFAQ DVGRMFKQFNKLTEDKADVQSIIGLQRFFETRMNEAFGDTKF	BL21(DE3)-R3-pRARE2

		SAVLVE	
WDR9(2)	gi|16445436	MHHHHHHSSGVDLGTENLYFQSMATNYVESNWKKQCKELVNL IFQCEDSEPFRQPVDLVEYPDYRDIIDTPMDFGTVRETLDAG NYDSPLEFCKDIRLIFSNAKAYTPNKRSKIYSMTLRLSALFE EKMKKISSDFKIGQKFNE	BL21(DE3)-R3-pRARE2

Supplementary Table 2 | Protein stability shift data for human bromodomains in the presence of JQ1. Observed Temperature Shift (ΔT_m^{obs}) of the thermal melting of human BET family members in the presence of **(+)-JQ1** or **(-)-JQ1** stereoisomer. Experiments were carried out in 10 mM HEPES pH 7.5 at 25 ^{o}C, 100 mM NaCl, using protein at a final concentration of 2 μM and ligands at 10 μM. SYPRO-Orange was added as a fluorescence probe. Excitation as well as emission was set to 465 nm and 590 nm, respectively. A temperature step of 3 ^{o}C per 1 min from 25 ^{o}C to 96 ^{o}C was applied. The sloping baselines of the initial and final fluorescent species with increasing temperature were approximated by a linear fit.

Protein	JQ1 (racemic)		(-)-JQ1		(+)-JQ1	
	ΔT_m^{obs}	STD	ΔT_m^{obs}	STD	ΔT_m^{obs}	STD
ASH1L	-	-	0.00	0.00	0.00	0.00
ATAD2	0.00	0.00	0.31	0.23	0.18	0.68
BAZ2B	0.00	0.00	0.00	0.00	0.00	0.00
BRD1	0.55	0.35	0.59	0.73	0.00	0.00
BRD2(1)	7.05	0.47	0.89	0.60	6.47	0.09
BRD2(2)	7.60	0.71	0.91	0.06	7.97	0.01
BRD3(1)	8.64	0.71	1.95	0.23	8.27	0.11
BRD3(2)	9.46	0.91	2.14	0.47	8.39	0.01
BRD4(1)	10.03	0.02	1.12	0.09	9.35	0.07
BRD4(2)	7.79	0.53	0.21	0.11	7.44	0.14
BRD9	0.00	0.00	0.00	0.00	0.00	0.00
BRDT(1)	4.21	0.97	0.38	0.02	3.93	0.13
BRPF1	1.05	0.62	0.76	0.18	0.00	0.00
CECR2	0.00	0.00	0.00	0.00	0.00	0.00
CREBBP	0.71	0.64	1.18	0.21	1.04	0.11
EP300	1.13	0.42	0.46	0.22	0.07	0.21
FALZ	0.00	0.00	0.00	0.00	0.00	0.00
GCN5L2	0.13	0.14	0.00	0.00	0.00	0.00
KIAA1240	0.00	0.00	0.14	0.22	0.05	0.28
LOC93349	0.27	1.07	0.00	0.00	0.00	0.00
PB1(1)	0.00	0.00	0.00	0.00	0.00	0.00
PB1(2)	0.00	0.00	0.48	0.11	0.00	0.00
PB1(3)	0.00	0.00	0.98	0.01	0.79	0.05
PB1(5)	0.20	0.71	0.37	0.25	0.00	0.00
PB1(6)	0.00	0.00	0.00	0.00	0.00	0.00
PCAF	0.00	0.00	0.00	0.00	0.00	0.00

PHIP(2)	1.35	0.54	0.00	0.00	0.00	0.00
SMARCA2	0.07	0.03	0.95	0.04	0.93	0.02
SMARCA4	0.00	0.00	0.60	0.18	0.15	0.10
SP140	0.00	0.00	0.69	0.80	0.00	0.00
TAF1(1)	0.00	0.00	0.56	0.04	0.28	0.05
TAF1(2)	0.56	0.64	0.33	0.03	0.50	0.04
TAF1L(1)	0.00	0.00	0.00	0.00	0.04	0.04
TAF1L(2)	0.77	0.05	0.14	0.18	0.00	0.00
TIF1	0.86	0.97	0.00	0.00	0.00	0.00
TRIM28	0.00	0.00	0.00	0.00	0.00	0.00
WDR9(2)	1.79	0.03	0.00	0.00	0.00	0.00

Supplementary Table 3 | Isothermal Titration Calorimetry of human BET family members and WDR9(2) or CREBBP (P) with (+)-JQ1 (L). Titrations were carried out in 50 mM HEPES pH 7.4 at 25 ^{o}C, 150 mM NaCl and 15 ^{o}C while stirring at 295 rpm. Protein concentration was between 250 - 300 µM (or 950 µM for CREBBP) and ligand concentration was between 25-30 µM as indicated in the table. In all cases the protein was titrated into the ligand solution (reverse titration).

Protein	[P] (µM)	[L] (µM)	K_d (nM)	ΔH^{obs} (kcal/mol)	N	$T\Delta S$ (kcal/mol)	ΔG (kcal/mol)
BRD2(1)	225	25	128.4 ± 6.5	-7.74 ± 0.003	1.02 ± 0.002	1.35	-7.74
BRD3(1)	306	25	59.5 ± 3.1	-6.57 ± 0.017	1.07 ± 0.002	2.97	-6.57
BRD3(2)	280	30	82.0 ± 5.3	-4.93 ± 0.017	1.03 ± 0.002	4.41	-4.93
BRD4(1)	240	25	49.0 ± 2.4	-8.42 ± 0.019	1.00 ± 0.001	1.22	-8.42
BRD4(2)	250	27	90.1 ± 4.6	-3.22 ± 0.009	1.06 ± 0.002	5.76	-3.22
BRDT(1)	305	25	190.1 ± 7.6	-8.30 ± 0.024	1.06 ± 0.002	0.56	-8.30
CREBBP	950	30	NA	NA	NA	NA	NA
WDR9(2)	300	25	NA	NA	NA	NA	NA

Supplementary Table 4 | Data collection and refinement statistics (molecular replacement). BRD4(1) apo structure, BRD4(1)/(+)-JQ1 complex and BRD2(2)/(+)-JQ1 complex.

	BRD2(2)/(+)-JQ1 (I)	**BRD4(1) (II)**	**BRD4(1)/(+)-JQ1 (III)**
Data collection			
Space group	$P2_12_12$	$P2_12_12_1$	$P2_12_12_1$
Cell dimensions			
a, *b*, *c* (Å)	52.57, 71.78, 31.92	37.41, 44.14, 78.41	36.80, 44.76, 78.39
α, β, γ (°)	90.00, 90.00, 90.00	90.00, 90.00, 90.00	90.00, 90.00, 90.00
Resolution (Å)	29.16 (1.61)	50.0 (1.35)	26.83 (1.60)
R_{merge}	0.055 (0.240)	0.071 (0.177)	0.046 (0.137)
$I/\sigma I$	16.1 (5.9)	30.2 (11.1)	18.6 (6.9)
Completeness (%)	99.5 (97.0)	99.9 (100.0)	99.7 (98.5)
Redundancy	3.4 (3.1)	8.1 (6.5)	4.1 (3.6)
Refinement			
Resolution (Å)	1.61	1.35	1.60
No. reflections	15342	29262	16715
R_{work}/ R_{free}	14.8 / 18.4	15.0 / 17.4	14.9 / 18.4
No. atoms			
Protein	924	1105	1074
Ligand/ion	41	12	48
Water	175	226	208
B-factors			
Protein	10.79	10.21	12.15
Ligand/ion	12.04	25.43	13.73
Water	24.77	24.47	23.67
R.m.s deviations			
Bond lengths (Å)	0.016	0.009	0.015
Bond angles (°)	1.724	1.298	1.698

Number of crystals for each structure should be noted in footnote.
*Highest resolution shell is shown in parenthesis.

Supplementary Table 5 | Summary of JQ1 binding studies performed against a panel of human recombinant ligand and ion receptors. JQ1 (1 μm) was screened against a panel of 55 ligand receptors, ion channels and transport proteins using an established and widely utilized commercial assay (ExpresSProfile; CEREP, Paris, FRANCE).

ASSAY	Catalogue Ref	% Inhibition of Contol Specific Binding	1st / % of Control Specific Inhibition	2nd / % of Control Specific Inhibition	Mean / % of Control Specific Binding	SEM % Control	Reference Compound	IC50 Ref. (M)	Ki Ref. (M)	nH Ref.
H2 (h) (antagonist radioligand)	1208	-27	127.0	127.0	127.0	0.0	cimetidine	1.70E-07	1.70E-07	0.6
NK3 (h) (antagonist radioligand)	104	-23	113.0	132.7	122.8	9.9	SB 222200	1.00E-08	5.60E-09	1.1
sst (non-selective) (agonist radioligand)	149	-22	120.5	123.5	122.0	1.5	somatostatin-14	2.10E-10	1.30E-10	0.7
BZD (central) (agonist radioligand)	28	-20	110.5	129.2	119.8	9.3	diazepam	1.20E-08	9.80E-09	0.9
TP (h) (TXA2/PGH2) (antagonist radioligand)	2048	-19	118.9	120.0	119.4	0.6	U 44069	1.30E-08	5.80E-09	0.9
5-HT transporter (h) (antagonist radioligand)	439	-19	109.0	128.1	118.6	9.5	imipramine	2.10E-09	9.60E-10	0.7
5-HT1A (h) (agonist radioligand)	131	-14	112.7	115.3	114.0	1.3	8-OH-DPAT	5.00E-10	3.10E-10	1.2
M1 (h) (antagonist radioligand)	91	-14	109.6	117.7	113.7	4.0	pirenzepine	9.00E-09	7.80E-09	0.9
GABA (non-selective) (agonist radioligand)	57	-12	115.1	108.3	111.7	3.4	GABA	2.40E-08	1.40E-08	0.7

5-HT7 (h) (agonist radioligand)	144	-12	108.2	114.9	111.5	3.3	serotonin	5.30E-10	2.00E-10	0.9
norepinephrine transporter (h) (antagonist radioligand)	355	-10	118.3	102.1	110.2	8.1	protriptyline	4.60E-09	3.40E-09	1.2
A1 (h) (antagonist radioligand)	2	-10	99.4	119.7	109.6	10.1	DPCPX	5.30E-10	3.30E-10	0.9
A2A (h) (agonist radioligand)	4	-9	110.9	107.3	109.1	1.8	NECA	2.60E-08	2.10E-08	0.7
VPAC1 (VIP1) (h) (agonist radioligand)	157	-9	110.3	107.0	108.7	1.6	VIP	1.40E-10	7.60E-11	0.9
dopamine transporter (h) (antagonist radioligand)	52	-7	108.6	106.0	107.3	1.3	BTCP	6.70E-09	3.60E-09	1.1
alpha 2 (non-selective) (antagonist radioligand)	11	-7	103.9	110.7	107.3	3.4	yohimbine	7.50E-08	3.20E-08	0.9
5-HT5a (h) (agonist radioligand)	140	-7	103.7	109.4	106.6	2.8	serotonin	1.50E-07	7.40E-08	0.8
delta 2 (DOP) (h) (agonist radioligand)	114	-6	97.5	115.2	106.3	8.9	DPDPE	2.40E-09	1.40E-09	0.9
5-HT3 (h) (antagonist radioligand)	411	-6	106.6	105.8	106.2	0.4	MDL 72222	5.80E-09	4.10E-09	1.0
CXCR2 (IL-8B) (h) (agonist radioligand)	419	-5	95.0	115.3	105.1	10.1	IL-8	8.60E-11	4.00E-11	1.3
alpha 1 (non-selective) (antagonist radioligand)	8	-5	105.6	104.1	104.9	0.8	prazosin	1.90E-10	5.00E-11	1.2
H1 (h) (antagonist radioligand)	870	-5	102.3	107.4	104.8	2.6	pyrilamine	2.20E-09	1.40E-09	1.0
V1a (h) (agonist radioligand)	159	-5	103.0	106.2	104.6	1.6	[d(CH2)51Tyr(Me)2]-AVP	8.60E-10	5.40E-10	1.0
Ca2+ channel (L verapamil site) (phenylalkylamine) (antagonist radioligand)	163	-5	101.2	107.9	104.5	3.3	D 600	6.80E-08	3.50E-08	0.6

CCR1 (h) (agonist radioligand)	361	-4	109.3	99.2	104.2	5.0	MIP-1alpha	5.00E-11	3.30E-11	0.7
mu (MOP) (h) (agonist radioligand)	118	-4	100.5	107.8	104.1	3.6	DAMGO	7.10E-10	2.90E-10	1.1
KV channel (antagonist radioligand)	166	-4	107.7	100.0	103.9	3.8	alpha -dendrotoxin	6.60E-10	5.30E-10	1.4
5-HT1B (antagonist radioligand)	132	-4	109.0	98.7	103.8	5.1	serotonin	1.50E-08	9.30E-09	0.7
M3 (h) (antagonist radioligand)	95	-4	100.4	107.0	103.7	3.3	4-DAMP	4.50E-10	3.20E-10	1.1
NTS1 (NT1) (h) (agonist radioligand)	109	-4	108.8	98.6	103.7	5.1	neurotensin	6.00E-10	4.90E-10	1.0
B2 (h) (agonist radioligand)	33	-3	100.6	105.5	103.0	2.4	NPC 567	2.00E-08	1.00E-08	0.8
NOP (ORL1) (h) (agonist radioligand)	358	-2	98.8	105.8	102.3	3.5	nociceptin	1.80E-09	9.00E-10	1.4
D1 (h) (antagonist radioligand)	44	-2	100.8	103.7	102.2	1.5	SCH 23390	1.50E-10	6.00E-11	1.0
D2S (h) (antagonist radioligand)	46	-2	94.9	109.1	102.0	7.1	(+)butaclamol	1.90E-09	6.50E-10	1.1
Y1 (h) (agonist radioligand)	106	-2	98.9	104.7	101.8	2.9	NPY	1.50E-10	1.10E-10	0.5
5-HT2B (h) (agonist radioligand)	1333	-1	97.2	105.4	101.3	4.1	(ƴ)DOI	2.30E-09	1.20E-09	0.9
AT1 (h) (antagonist radioligand)	24	0	93.5	106.8	100.2	6.7	saralasin	5.20E-10	2.60E-10	0.6
CB1 (h) (agonist radioligand)	36	0	93.8	106.3	100.1	6.3	CP 55940	4.40E-10	3.80E-10	0.9
MC4 (h) (agonist radioligand)	420	0	99.1	101.0	100.0	1.0	NDP-alpha -MSH	1.60E-10	1.40E-10	0.7
beta 1 (h) (agonist radioligand)	18	1	96.5	101.8	99.2	2.6	atenolol	2.60E-07	1.90E-07	0.9
M2 (h) (antagonist radioligand)	93	2	94.1	101.5	97.8	3.7	methoctramine	1.90E-08	1.30E-08	0.7
5-HT6 (h) (agonist radioligand)	142	2	97.4	98.0	97.7	0.3	serotonin	1.20E-07	5.50E-08	0.8

Cl- channel (GABA-gated) (antagonist radioligand)	170	3	96.5	98.3	97.4	0.9	picrotoxinin	1.00E-07	8.50E-08	0.9
SKCa channel (antagonist radioligand)	167	3	93.9	99.9	96.9	3.0	apamin	5.00E-12	2.50E-12	0.6
kappa (KOP) (agonist radioligand)	1971	3	89.0	104.5	96.8	7.7	U 50488	6.30E-10	4.20E-10	1.0
beta 2 (h) (agonist radioligand)	20	4	94.9	98.1	96.5	1.6	ICI 118551	9.00E-10	3.00E-10	1.1
GAL2 (h) (agonist radioligand)	410	5	93.7	96.3	95.0	1.3	galanin	1.50E-09	1.40E-09	1.1
CCK1 (CCKA) (h) (agonist radioligand)	39	9	91.8	90.4	91.1	0.7	CCK-8s	1.60E-10	1.20E-10	1.3
Y2 (h) (agonist radioligand)	107	10	85.2	95.5	90.4	5.2	NPY	4.80E-10	1.90E-10	0.5
ETA (h) (agonist radioligand)	54	16	85.4	82.1	83.7	1.6	endothelin-1	3.40E-11	1.70E-11	1.2
Na+ channel (site 2) (antagonist radioligand)	169	18	78.4	85.4	81.9	3.5	veratridine	3.70E-06	3.30E-06	0.7
5-HT2A (h) (antagonist radioligand)	135	24	72.8	79.8	76.3	3.5	ketanserin	5.50E-10	3.00E-10	1.0
MT1 (ML1A) (h) (agonist radioligand)	1538	29	72.0	69.8	70.9	1.1	melatonin	2.10E-10	1.70E-10	1.0
NK2 (h) (agonist radioligand)	102	56	40.5	48.2	44.4	3.9	[Nleu10]-NKA (4-10)	1.50E-09	8.40E-10	0.7
A3 (h) (agonist radioligand)	6	61	26.1	52.4	39.3	13.1	IB-MECA	4.30E-10	2.60E-10	1.2
H2 (h) (antagonist radioligand)	1208	-27	127.0	127.0	127.0	0.0	cimetidine	1.70E-07	1.70E-07	0.6

References

44. Toretsky, J.A., *et al.* Translocation (11;15;19): a highly specific chromosome rearrangement associated with poorly differentiated thymic carcinoma in young patients. *Am J Clin Oncol* **26**, 300-306 (2003).
45. Kees, U.R., Mulcahy, M.T. & Willoughby, M.L. Intrathoracic carcinoma in an 11-year-old girl showing a translocation t(15;19). *Am J Pediatr Hematol Oncol* **13**, 459-464 (1991).
46. French, C.A., *et al.* BRD-NUT oncoproteins: a family of closely related nuclear proteins that block epithelial differentiation and maintain the growth of carcinoma cells. *Oncogene* **27**, 2237-2242 (2008).
47. This vector includes sites for ligation-independent cloning and a Tobacco Etch Virus (TEV)-cleavable N-terminal His6-tag (extension MHHHHHHSSGVDLGTENLYFQ*SM-) After digestion with TEV protease, the protein retains an additional serine and methionine on the N-terminus.
48. Stols, L., *et al.* A new vector for high-throughput, ligation-independent cloning encoding a tobacco etch virus protease cleavage site. *Protein Expression and Purification* **25**, 8-15 (2002).
49. Zhang, Z.Q. & Marshall, A.G. A universal algorithm for fast and automated charge state deconvolution of electrospray mass-to-charge ratio spectra. *Journal of the American Society for Mass Spectrometry* **9**, 225-233 (1998).
50. Wiseman, T., Williston, S., Brandts, J.F. & Lin, L.N. Rapid Measurement of Binding Constants and Heats of Binding Using a New Titration Calorimeter. *Analytical Biochemistry* **179**, 131-137 (1989).
51. Wigle, T.J., *et al.* Screening for inhibitors of low-affinity epigenetic peptide-protein interactions: an AlphaScreen-based assay for antagonists of methyl-lysine binding proteins. *J Biomol Screen* **15**, 62-71 (2010).
52. Leslie, A.G.W. & Powell, H. MOSFLM. (MRC Laboratory of Molecular Biology, Cambridge, 2007).
53. Evans, P. SCALA - scale together multiple observations of reflections. (MRC Laboratory of Molecular Biology, Cambridge, 2007).
54. Otwinowski, Z. & Minor, W. Processing of X-ray diffraction data collected in oscillation mode. in *Macromolecular Crystallography, Pt A*, Vol. 276 307-326 (Academic Press Inc, San Diego, 1997).
55. McCoy, A.J., Grosse-Kunstleve, R.W., Storoni, L.C. & Read, R.J. Likelihood-enhanced fast translation functions. *Acta Crystallographica Section D-Biological Crystallography* **61**, 458-464 (2005).
56. Perrakis, A., Morris, R. & Lamzin, V.S. Automated protein model building combined with iterative structure refinement. *Nat Struct Biol* **6**, 458-463 (1999).
57. Emsley, P. & Cowtan, K. Coot: model-building tools for molecular graphics. *Acta Crystallogr D Biol Crystallogr* **60**, 2126-2132 (2004).
58. Murshudov, G.N., Vagin, A.A. & Dodson, E.J. Refinement of macromolecular structures by the maximum-likelihood method. *Acta Crystallographica Section D-Biological Crystallography* **53**, 240-255 (1997).

59. Painter, J. & Merritt, E.A. Optimal description of a protein structure in terms of multiple groups undergoing TLS motion. *Acta Crystallogr D Biol Crystallogr* **62**, 439-450 (2006).
60. Shen, Y., *et al.* Blueprint for antimicrobial hit discovery targeting metabolic networks. *Proc Natl Acad Sci U S A* **107**, 1082-1087 (2010).
61. Case, D.A., *et al.* AMBER 10. (University of California, San Francisco, CA, USA, 2008).
62. Larkin, M.A., *et al.* Clustal W and Clustal X version 2.0. *Bioinformatics* **23**, 2947-2948 (2007).
63. Kedersha, N., Tisdale, S., Hickman, T. & Anderson, P. Real-time and quantitative imaging of mammalian stress granules and processing bodies. *Methods Enzymol* **448**, 521-552 (2008).
64. French, C.A. Demystified molecular pathology of NUT midline carcinomas. *J Clin Pathol* **63**, 492-496 (2010).
65. Tranberg, C.E., *et al.* 2-Amino-3-aroyl-4,5-alkylthiophenes: agonist allosteric enhancers at human A(1) adenosine receptors. *J Med Chem* **45**, 382-389 (2002).
66. Walser, A., *et al.* Triazolobenzo- and triazolothienodiazepines as potent antagonists of platelet activating factor. *J Med Chem* **34**, 1209-1221 (1991).